Laboratory experiments on the thermodynamics of melting sea ice

Master's Thesis in Meteorology

Mareike Wiese

Mentors:
Prof. Dr. Martin Claußen
Dr. Dirk Notz

Meteorologisches Institut
Department Geowissenschaften
Universität Hamburg

Hamburg, September 2012

Contents

List of Symbols

c_i	specific heat capacity of ice	J kg^{-1} K^{-1}
C	heat transfer coefficient	W m^{-2} °C^{-1}
h	ice thickness	cm
k_i	heat conductivity of ice	W m^{-1} K^{-1}
k_{ic}	heat conductivity of ice crystals	W m^{-1} K^{-1}
k_{br}	heat conductivity of brine	W m^{-1} K^{-1}
L_i	latent heat of fusion of ice	J kg^{-1}
m_i	mass of ice	kg
p	pressure	Pa
q	internal heat sources	W m^{-3}
Q_a	atmospheric heat flux	W m^{-2}
Q_c	conductive heat flux through the ice	W m^{-2}
$Q_{c,b}$	conductive heat flux at the bottom of the ice	W m^{-2}
$Q_{c,t}$	conductive heat flux at the top of the ice	W m^{-2}
Q_L	latent heat flux	W m^{-2}
Q_w	oceanic heat flux	W m^{-2}
R	resistance	Ω

RP	reduction parameter	
S	initial water salinity	g kg^{-1}
S_{bu}	bulk salinity	g kg^{-1}
S_{br}	brine salinity	g kg^{-1}
t	time of ice growth	h
T	temperature	°C
T_a	air temperature	°C
T_{ag}	air temperature during ice growth	°C
T_{am}	air temperature during melting	°C
T_f	freezing temperature	°C
T_i	ice temperature	°C
T_m	melting point of ice	°C
T_s	ice-surface temperature	°C
T_{sam}	set air temperature for melting	°C
$T_{\rho max}$	temperature at maximum seawater density	°C
ΔT	difference between ice temperature and melting point	°C
Δh	thickness of the growing/melting ice	cm
ρ_i	density of ice	kg m^{-3}
ϕ	solid fraction	

Abstract

During the last decades a strong decrease in Arctic sea-ice extent has been observed, which has not been forecasted as strongly by climate models. To better understand the underlying cause of this discrepancy, laboratory experiments were performed to get a better understanding of the thermodynamics of melting sea ice. To clarify the influence of the salt within sea ice, freshwater ice and sea ice is compared.

The measurements reveal that sea ice melts faster than freshwater ice of the same thickness. Moreover, sea ice melts faster in turbulent water than in calm water. For a constant air temperature, the meltrate of freshwater ice is constant with time, whereas the melt rate of sea ice shows a distinct maximum. A model study shows that this maximum occurs earlier at higher atmospheric heat fluxes.

After increasing the air temperature, freshwater ice warms faster than sea ice. Moreover, freshwater ice warms uniformly until reaching the melting point over the whole depth, whereas in sea ice, a non-linear temperature profile develops. The bottom melting of sea ice is stronger than that of freshwater ice. Additionally, the melting at the sea-ice bottom increases with time, which fits well to the increase in the melt rate. During one of the sea-ice experiments, a strong short-term flushing event was likely observed.

During melting, very small melt ponds developed on the sea-ice surface. The measured ice-surface temperature was higher than the melting point, independent of salinity. The surface temperature of sea ice decreases with an increasing salinity and increases with an increasing air temperature.

Abstract

Chapter 1

Introduction

1.1 Motivation

In terms of its volume, sea ice is a rather small part of the cryosphere, which includes all frozen water on earth, e.g. glacier ice, snow and the ice in frozen grounds. The volume of sea ice is estimated to be only 0.2 % of the volume of glacier ice, because sea ice only reaches thicknesses of a few meters. On the other hand, sea ice covers approximately 7.3 % of the Earth's surface and 11.8 % of the total ocean surface (*Weeks*, 2010).

Sea ice plays an important role in the Earth's climate system. Sea ice insulates the relatively warm ocean from the cold atmosphere and thus affects the heat and water vapour exchange at the ocean-atmosphere interface. Moreover, sea ice influences the water masses below the ice due to salt loss during growth and freshwater input during melting which influences water currents (*Stössel et al.*, 2002). Another important property of sea ice is the high albedo of approximately 0.8 (cold bare ice) to 0.9 (snow-covered ice) (*Weeks*, 2010). As a result, much more incoming shortwave radiation is reflected by sea ice than by ocean water which has a lower albedo. Furthermore, sea ice also plays a critical role as the habitat of some marine plants and animals including

micro-organisms, birds and mammals.

Sea ice is coupled to the atmosphere and ocean by thermodynamic (growth/decay) and dynamic (drift) processes. Thin sea ice reacts quickly to changes in the air and ocean. Probably the most important change during the last decades has been the increasing global air temperature that especially affects the Arctic due to feedbacks and interactions with sea ice and snow cover (*Serreze and Francis*, 2006). Such a positive feedback is the 'ice-albedo-feedback'. Due to higher air temperatures the sea-ice cover decreases which reveals more open ocean water. Since water has a lower albedo than sea ice, water absorbs more incoming solar radiation, which results in increasing water and air temperatures. These higher temperatures again increase ice melting and so on. This feedback was quite noticeable during the last three decades. A strong decrease in sea-ice extent was observed in the Arctic, which Figure 1.1 clearly shows. The year 2007 is not even included in this figure. In that year, the far lowest ice extent to date (4.28×10^6 km^2) was observed (*Weeks*, 2010). Moreover, a reduction in sea-ice thickness was observed as well.

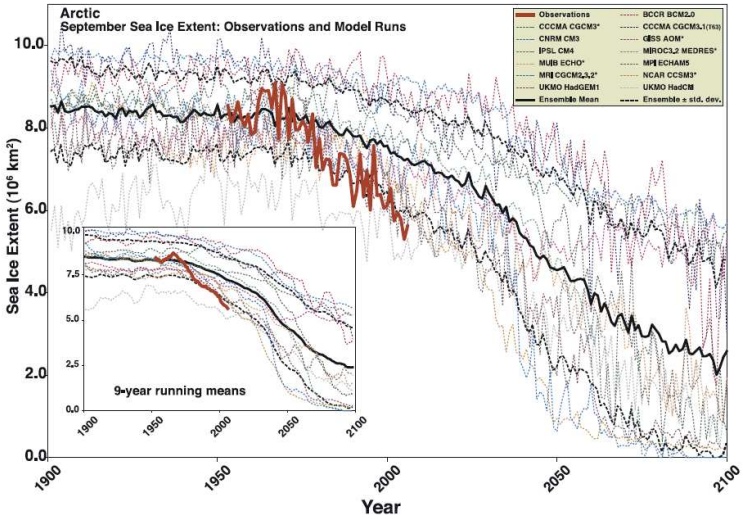

Figure 1.1: *Arctic September sea-ice extent from observations (thick red line, 1953 to 2006) and 13 IPCC AR4 climate models (dotted coloured lines), together with the multi-model ensemble mean (solid black line) and standard deviation (dotted black line). The inset shows the same data presented using a nine-year running mean (Stroeve et al., 2007).*

Figure 1.1 shows the Arctic September sea-ice extent, which is at the end of the melt season, from satellite observations and results from 13 of the IPCC Fourth Assessment

Report (IPCC AR4) models. All models agree that the ice extent will decrease within the next decades associated with the warming in the Arctic. But in comparison with the observations, the recent changes in September sea-ice extent are much stronger than forecasted by the models (*Stroeve et al.*, 2007). This difference between observations and model results raises the question of how well models could predict the changes in the sea-ice extent. The year 2007 is a good example of how complex the air-ice-ocean interactions are in the Arctic. Atmospheric pressure patterns can influence the cloud cover which in turn affects the incoming solar radiation and thus the ocean water temperature and ice melting. Moreover, the ice circulation is also affected by the atmospheric pressure patterns, which influences the ice transport out of the Arctic. Higher ocean water temperatures can enhance the melting at the bottom and sides of the ice. Additionally, the ice thickness has an effect on the ice melting and the ice transport (*Weeks*, 2010). It could be that those complex air-ice-ocean interactions and/or the melting process of sea ice itself are not fully understood and/or not represented in the models yet. To investigate one possible reason for the discrepancy between model results and observations, tank experiments were carried out to get a better understanding of how sea ice melts.

There have been only a few field studies of melting sea ice, which focused mainly on the evolution of the meltwater, the ice surface and the ice salinity. *Holt and Digby* (1985) did observations of the melting process in first-year ice with both radar and visual imagery from aircraft and satellite. They found that the topography of the ice increased due to the drainage of meltwater. Moreover, they found a desalination zone in the upper part of the ice due to flushing. *Eicken et al.* (2002) did a tracer study to find out more about meltwater transport on and in sea ice. They found different stages of melting. The formation and evolution of melt ponds at the ice surface depended on the meltwater supply and the ice permeability. *Widell et al.* (2006) investigated the salt release from warming sea ice in a field study in the Arctic. They observed dense saline plumes under melting land-fast first-year ice due to brine convection within the warm permeable ice. The downward salt flux correlated well with an upward oceanic heat flux. *Tison et al.* (2008) found that internal melting increases the porosity of warming first-year sea ice, which favours a decrease in bulk salinity by downward brine migration. The drainage process stops after some time due to a lower brine salinity than the sea-water salinity. *Tison et al.* (2008) indicate that these processes influence the biogeochemical evolution of the ice.

There have been several experimental studies on sea ice in tanks, which focused mainly on sea-ice growth. For example, *Naumann* (2011) analysed the sea-ice growth in calm water and disturbed water. So far the thermodynamics of melting sea ice have not been investigated in field studies or in tank experiments. Therefore, the experiments that

were performed in the context of this thesis are the first ones of this type.

1.2 Outline of the thesis

With the help of the laboratory experiments, it will be analysed how fast sea ice melts and how the melt rate depends on salinity and on the atmospheric and oceanic heat flux. Therefore, a closer look into detailed ice temperature profiles is done. The measurements are compared to results from a thermodynamic sea-ice model (*Griewank and Notz*, submitted). Moreover, it is investigated how the ice-surface temperature depends on ice thickness, salinity and air temperature. A theoretical background about the thermophysical properties and the thermodynamics of sea ice is given in Chapter 2. The laboratory experiments were performed in a tank inside a cold room. The setup of the tank and the experimental setup are described in Chapter 3. The results of the measurements are presented in Chapter 4. In Chapter 5, the results and possible improvements of the experiments are discussed.

Chapter 2

Theoretical background

2.1 Thermophysical properties of seawater

Seawater freezes at lower temperatures than freshwater due to the salinity. The freezing point T_f and the temperature at the maximum density $T_{\rho max}$ of seawater depend on the seawater's salinity (Figure 2.1). Both decrease with increasing salinity. At a salinity of 24.65 g kg^{-1} both temperatures are equal to -1.34 °C. At lower salinities the temperature at maximum density is higher than the freezing point and vice versa at higher salinities. Seawater usually has higher salinities than 24.65 g kg^{-1}. The high salinities imply that convective mixing occurs due to cooling until the water is cooled down for several meters. Only then ice growth becomes possible.

The freezing point of water T_f can be calculated by the following equation 2.1 (*Fofonoff and Millard,* 1983):

$$T_f = -0.0575S + 0.0017S^{\frac{3}{2}} - 0.0002S^2 - 0.0007p^4 \tag{2.1}$$

S corresponds to the water salinity and p to the pressure.

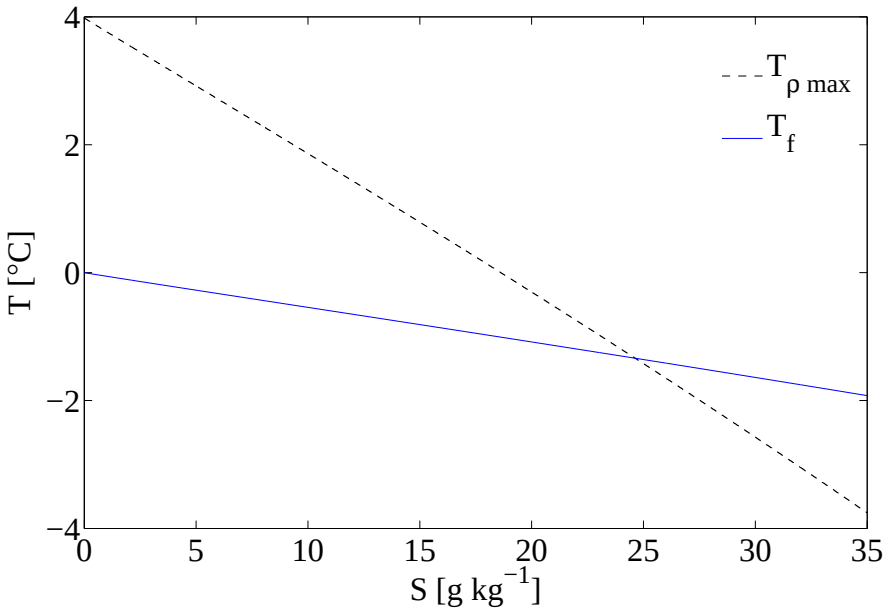

Figure 2.1: *Freezing point T_f and temperature at maximum density $T_{\rho max}$ of sea water as a function of salinity S.*

2.2 Thermophysical properties of sea ice

When ice grows within seawater, salt gets entrapped in brine inclusions in between the ice crystals that consist of pure ice. Therefore, sea ice is called a mushy layer, since sea ice has two main components (ice and salt) and two phases (solid and liquid) (*Feltham et al.*, 2006). Only at very low temperatures around -40°C, sea ice becomes a completely solid mixture of pure ice and salts (*Schwerdtfeger*, 1963). This complex composition of sea ice influences its physical properties during freezing and melting. The heat capacity, the heat conductivity and the latent heat of fusion of sea ice depend on the bulk salinity and temperature of the ice (Figure 2.2).

The heat capacity of sea ice is composed of the heat capacity of its different components. Additionally, the heat capacity includes the energy that is needed to internally melt the ice. To maintain thermal equilibrium when sea ice warms, the brine salinity has to be reduced by melting the freshwater ice crystals. The heat capacity of sea ice c_i can be calculated as follows (*Notz*, 2005):

$$c_i = 2112.2 + 7.6973T_i + 18046\frac{S_{bu}}{T_i^2} \tag{2.2}$$

T_i corresponds to the ice temperature and S_{bu} to the bulk salinity.

The heat conductivity k_i can be calculated by the following equation (*Notz*, 2005):

$$k_i = \phi \cdot k_{ic}(T_i) + (1 - \phi) \cdot k_{br}(T_i, S_{br}) \tag{2.3}$$

The parameters k_{ic} and k_{br} correspond to the heat conductivities of the ice crystals and the brine, respectively. k_{ic} only depends on the ice temperature T_i whereas k_{br} additionally depends on the brine salinity S_{br}. The brine salinity can be calculated with the liquidus relationship:

$$S_{br} = -\frac{T_i}{0.05411}$$

Hence, k_{ic} and k_{br} result from the following equations:

$$\begin{aligned} k_{ic}(T_i) &= 2.21 - 1 \cdot 10^{-2} T_i + 3.44 \cdot 10^{-5} T_i^2 \\ k_{br}(T_i, S_{br}) &= 0.52325 \cdot \left(1 - \frac{S_{br}}{10^3}\right) + 0.01256 T_i + 5.8604 \cdot 10^{-5} T_i^2 \end{aligned}$$

The solid mass fraction ϕ describes the fraction of the solid ice crystals within sea ice and can be obtained from the bulk and brine salinity S_{bu} and S_{br}:

$$\phi = 1 - \frac{S_{bu}}{S_{br}}$$

According to *Weeks* (2010) the latent heat of fusion L_i can be calculated by:

$$L_i = 333.4 - 2.113 T_i - 0.114 S_{bu} + 18.04 \frac{S_{bu}}{T_i} \tag{2.4}$$

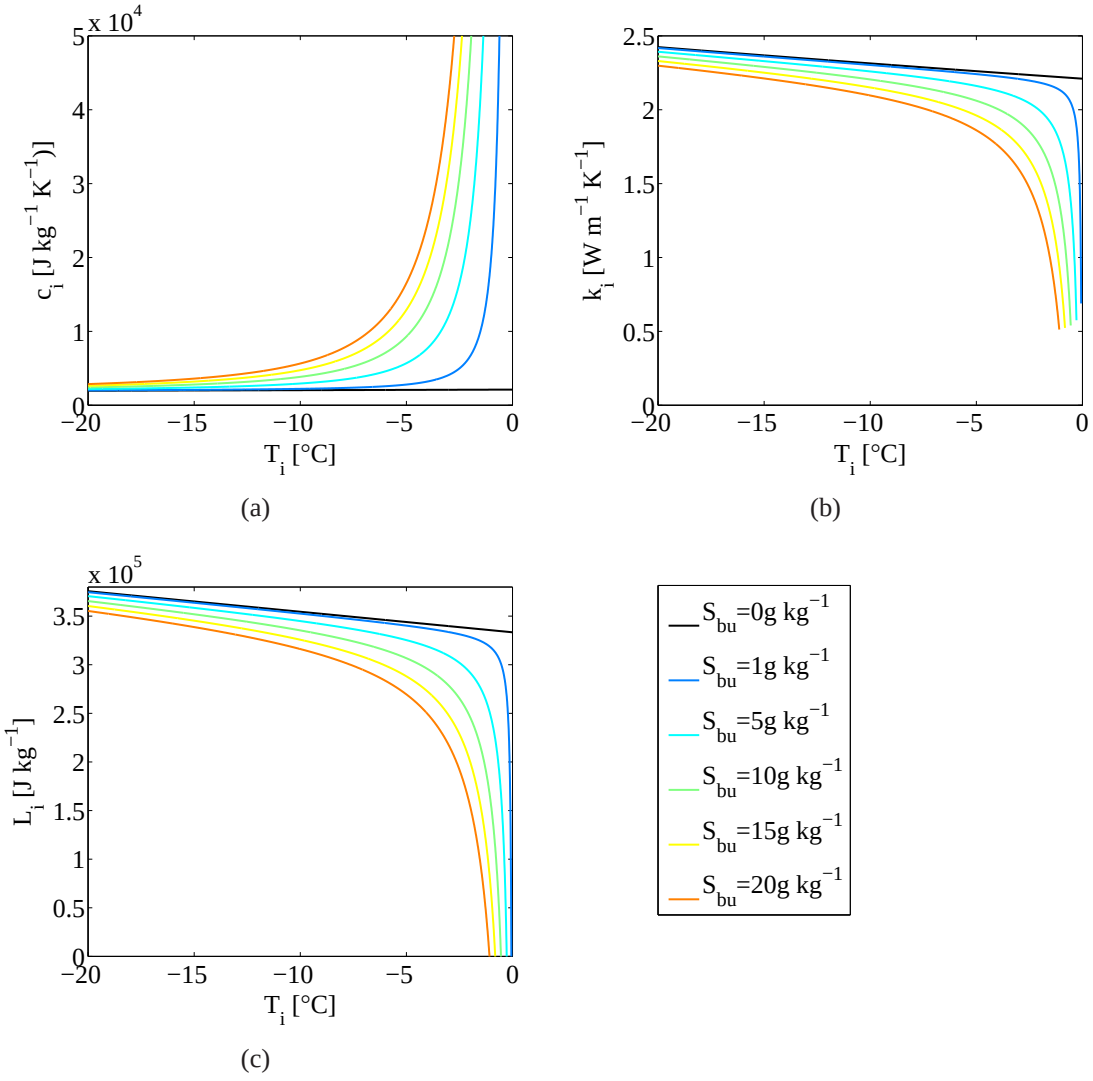

Figure 2.2: *Heat capacity of ice c_i (a), heat conductivity of ice k_i (b) and latent heat of fusion of ice L_i (c) as a function of the ice temperature T_i and the bulk salinity S_{bu}.*

2.3 Thermodynamics of sea ice

The thermodynamics of sea ice can be described by the heat conduction equation:

$$\rho_i \frac{\partial}{\partial t} c_i T_i = \nabla(k_i \nabla T_i) + q = \nabla Q_c + q \tag{2.5}$$

T_i corresponds to the ice temperature, ρ_i to the ice density, c_i to the heat capacity of the ice and k_i to the heat conductivity of the ice. The term on the left side of Equation 2.5 describes the cooling or warming of the ice which is due to a gradient in the conductive heat flux Q_c and internal heat sources q, i.e. solar radiation penetrating into the ice (*Leppäranta*, 1993).

Horizontal gradients in sea ice are small compared to vertical gradients. Hence, in sea ice heat is primarily exchanged in the vertical direction and Equation 2.5 can be simplified to a 1-D approach:

$$\rho_i \frac{\partial}{\partial t} c_i T_i = \frac{\partial Q_c}{\partial h} + q \tag{2.6}$$

h corresponds to the ice thickness.

Ice growth and melting depend on the atmospheric and oceanic heat flux Q_a and Q_w. Figure 2.3 illustrates the heat fluxes during ice growth according to the 1-D approach. Positive heat fluxes are directed upwards. $Q_{c,t}$ and $Q_{c,b}$ correspond to the conductive heat fluxes on the top and bottom of the ice, respectively. Q_L corresponds to the latent heat due to ice growth.

To calculate ice growth using Stefan's law, additional assumptions must be made. Thermal inertia is assumed to be neglected ($c_i = 0$), which leads to a linear temperature profile in the ice as shown in Figure 2.3. The ice bottom is at the freezing point of the water below the ice and the top of the ice is assumed to have the same temperature as the air directly above the ice. Assuming further that no solar radiation goes into the ice, the heat conduction is constant throughout the whole ice layer:

$$\begin{aligned} c_i = 0 \quad &\Rightarrow \quad \frac{\partial}{\partial t} \rho_i c_i T_i = 0 \\ q = 0 \quad &\Rightarrow \quad \frac{\partial Q_c}{\partial h} = 0, \\ &\qquad Q_{c,t} = Q_{c,b} \end{aligned}$$

The conductive heat flux is equal to the atmospheric heat flux at the top and equal to the latent and oceanic heat flux at the bottom of the ice. Hence, the ice growth balances the

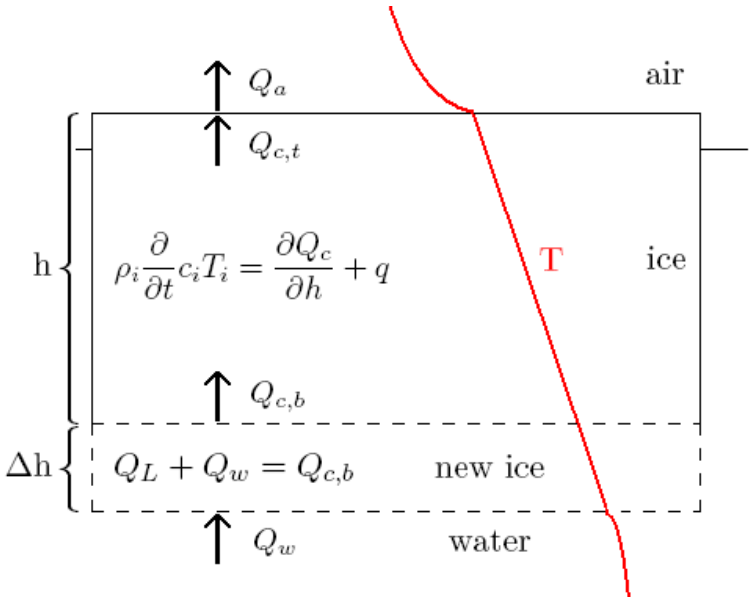

Figure 2.3: *Heat fluxes during ice growth (1D-approach). Q_a: atmospheric heat flux, Q_c: conductive heat flux through the ice, $Q_{c,t}$: conductive heat flux at the top of the ice, $Q_{c,b}$: conductive heat flux at the bottom of the ice, Q_L: latent heat, Q_w: oceanic heat flux, h: ice thickness, Δh: thickness of growing ice, ρ_i: ice density, c_i: heat capacity of the ice, T: temperature, T_i: ice temperature, q: internal heat sources.*

atmospheric and oceanic heat flux (*Leppäranta*, 1993):

$$\begin{aligned} Q_{c,t} &= Q_a \\ Q_L + Q_w &= Q_{c,b} \\ \rho_i L_i \frac{dh}{dt} + Q_w &= k_i \frac{\partial T_i}{\partial h} \end{aligned} \tag{2.7}$$

L_i corresponds to the latent heat of fusion of the ice and h corresponds to the ice thickness. Neglecting the oceanic heat flux, Equation 2.7 becomes the Stefan's law, with which the evolution of the ice thickness can be calculated.

The knowledge about thermodynamics of sea ice melting is rather sparse, in contrast to freshwater ice melting, which consists of two steps. First, the ice needs to be warmed with the energy $E_w = c_i m_i \Delta T$. ΔT corresponds to the temperature difference between the current ice temperature and the melting point and m_i corresponds to the mass of the ice. When the ice temperature reaches the melting point, which is 0°C for freshwater ice, it needs the energy $E_m = L_i m_i$ to melt.

Due to the complex composition of sea ice, the melting proceeds differently. When

the ice temperature increases, the freshwater-ice crystals melt and the brine becomes less saline to keep the thermal equilibrium, and conversely for decreasing temperatures. Therefore, with each temperature change some internal melting occurs. When sea ice warms it gets more and more liquid until it is completely liquid (*Feltham and Worster*, 2000). The melting temperature of sea ice depends on the bulk salinity and can be calculated from the liquidus relationship. For high temperatures close to the freezing point of seawater with low salinity, a linear fit provides a good approximation (*Notz*, 2005):

$$T_m = -0.05411 \cdot S_{bu} \tag{2.8}$$

T_m corresponds to the sea-ice melting temperature and S_{bu} corresponds to the bulk salinity.

The bulk salinity, which is defined as grams of salt per kilogram of sea ice (freshwater ice crystals plus brine), does not stay constant. Due to two main processes, sea ice loses salt. During ice growth, 'gravity drainage' causes the largest salt loss. When the air temperature increases and snow on top of the ice and the ice itself start to melt, so-called 'flushing' replaces brine with fresh meltwater from the surface (*Notz*, 2005). Since the bulk salinity of sea ice varies with depth (*Weeks*, 2010), the physical properties of sea ice are not constant with depth.

Chapter 3

Experiments

To investigate the melting of sea ice, laboratory experiments were performed in a tank inside a cold room in two periods with a changing setup. In the first period, eleven experiments were performed. The first two of these experiments were used to test the growth of freshwater ice in the tank and to examine the feasibility of measurements on melting sea ice. During the other experiments of the first period, 10 cm thick ice was grown and melted subsequently under varying conditions. In the second period, seven further experiments were performed. Here, ice thicker than 10 cm was grown and warmed slowly to analyse the salt loss of warming and melting sea ice. In the present study, the analysis is focused on the experiments of the first period of measurements.

In this chapter the performed laboratory experiments are presented. Section 3.1 describes the setup of the tank followed by a detailed description of the experiments in Section 3.2. In Section 3.3 several instruments used for the measurements and their calibration are presented in more detail.

3.1 Setup of the tank

The tank used for the experiments is 1.94 m long and 0.66 m wide. The water height of the experiments varied between 82.5 cm and 93.5 cm depending on the ice thickness that was planned to grow. The water level was higher for thicker ice. In order to obtain seawater, freshwater was filled into the tank and mixed with sea salt (Reef Excel Lab Marine Salt). The walls and the bottom of the tank are thermally insulated with 5 cm thick styrofoam plates to ensure that heat is exchanged only through the air-water-interface or air-ice-interface. To avoid ice freezing on the walls and keep it afloat, heating plates of 23 cm height are installed at the level of the water surface. These heating plates are inserted between the glass walls of the tank and the styrofoam plates. The air inside the cold room can be cooled down to -25°C.

Figure 3.1 (a) and Figure 3.2 show the setup of the instruments for the first period of experiments. The measurements were primarily done in the right part of the tank since the ice was slightly thicker there than in the left part of the tank. In the right part of the tank slightly lower temperatures were observed which might result from the airflow from the cooling machine and which might have been the reason for the thicker ice there. The ice thickness was measured with a ruler frozen into the ice which was visible through a small gap between the heating plates. The interval between ice thickness measurements varied between experiments and also between ice growth and melting. During ice growth the ice thickness was measured mostly every two to three hours. During melting, the ice thickness was measured hourly.

The ice temperature was measured with two thermistor chains of different length by measuring the resistance of the thermistors. Each thermistor chain had a counterweight to prevent the ice from being pulled underneath the water surface by the weight of the thermistor chain, especially during melting. Both thermistor chains consist of 29 thermistors. The thermistors on the long chain were placed equidistantly with a spacing of 3 cm. The short thermistor chain had a different arrangement of the thermistors: the first ten were placed with gaps of 0.5 cm, the next five with gaps of 1 cm, and the last four thermistors had distances of 2 cm. The first thermistor of the short chain did not work. Only the first working thermistor of the short chain was in the air, so that the thermistors with the smaller spacing were in the ice, but also the air temperature directly above the ice could be measured with the top thermistor. A couple of thermistors of the long chain were also in the air so that the thermistors measured air, ice and water temperature. The measurements were recorded for both thermistor chains every 10 seconds by a logger (Campbell CR3000 Micrologger).

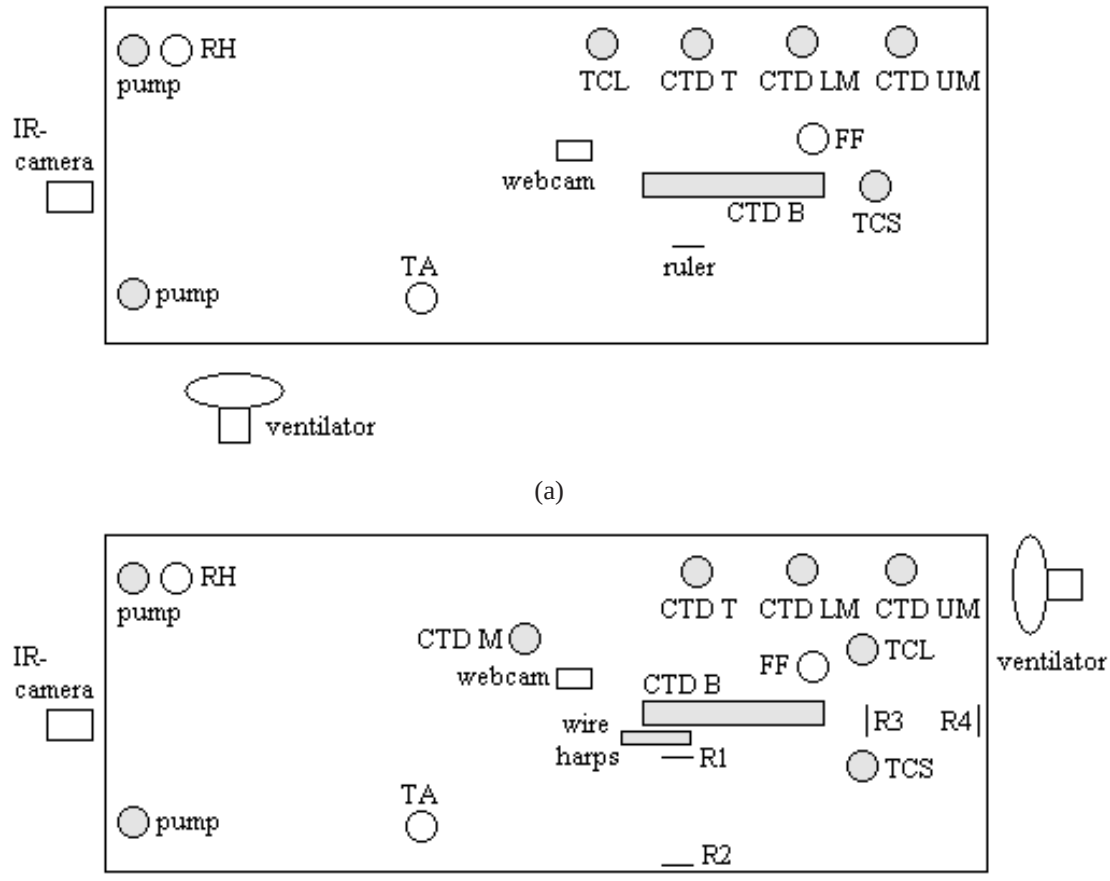

Figure 3.1: *Setup of the tank (top view) during the first period (a) and the second period as an example for the experiments with more than 10 cm thick ice (b). RH: relative humidity sensor, TA: air temperature sensor, FF: wind speed sensor, IR-camera: Infrared camera, TCL: long thermistor chain, TCS: short thermistor chain, CTD T: CTD top, CTD UM: CTD upper middle, CTD LM: CTD lower middle, CTD B: CTD on the bottom, CTD M: moveable CTD, R1-R4: rulers 1-4.*

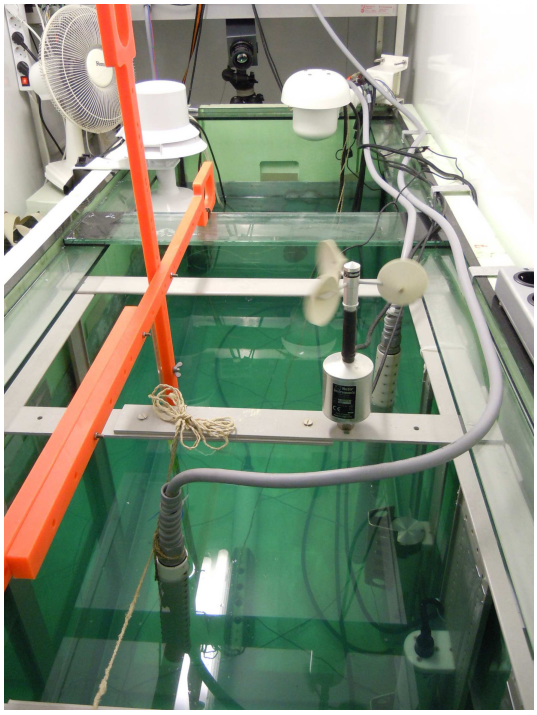

Figure 3.2: *Photo of the tank during the first period of measurements. View from the right side of the tank.*

Four CTDs (‘conductivity, temperature, depth’, SBE 37-SM MicroCAT) were installed at different heights to measure the salinity and the temperature of the water, except for the freshwater experiments. The lowest CTD always lay on the bottom so that the sensor on the CTD measured 9 cm above the tank bottom. The other three CTDs were installed on a frame at the back wall. The heights varied slightly with the changing water levels between the experiments. The sensors of the uppermost CTD, the CTD in the upper middle and the CTD in the lower middle were located at 15.5 cm to 17.5 cm, 24.5 cm to 26.5 cm and 63.5 cm to 65.5 cm water depth, respectively. All CTDs recorded measurements every 10 seconds. Furthermore, the CTDs were used to get the right salinity of the water when the sea salt was mixed into the freshwater. The measured salinity was lower than calculated from the definition of the water salinity, which corresponds to grams of salt per grams of seawater (salt + freshwater). This difference occurred due to crystallization water, which accounts for 10 to 15 % of the weight of the salt. Therefore, a larger amount of salt was added to the water than calculated until the CTDs measured the required salinity.

A heating wire was installed on the bottom of the tank to represent the oceanic heat flux. On the left part of the tank, two pumps were placed 24 cm to 28 cm below the

water surface in order to keep the water mixed during melting in some experiments as well as during the cooling of the water before starting a new experiment. A heating wire was winded around the pumps in order to keep them free from floating ice crystals.

Around 38 cm and 20 cm above the ice, a relative humidity sensor (Rotronic hygrometer MP100A) and a temperature sensor (Young platinum temperature probe, model 41342) were installed. The temperature sensor was used to measure the exact air temperature inside the cold room. Even though the temperature could be controlled with a thermostat, the real air temperature inside the cold room always differed a bit from that set value. Additionally, the cooling system had to stop approximately every six hours to warm and get ice-free again. Furthermore, a wind speed sensor (Vector Instruments anemometer A100R) was installed around 48 cm above the ice. A ventilator was placed next to the tank at the height of the tank rim to mix the air inside the cold room during melting to ensure turbulent conditions above the ice and to avoid an accumulation of cold air inside the tank directly above the ice. The wind speed sensor was primarily used to check after an experiment whether and when the ventilator was turned on. The data from the temperature sensor, the relative humidity sensor and the wind speed sensor were recorded every 30 seconds by a second logger (Campbell CR3000 Micrologger).

Two different cameras were used to observe the ice surface. A small webcam installed above the middle of the tank was directed onto the right part of the tank, where the measurements were done. Every three minutes a picture was taken automatically. This camera was used to observe changes in the structure of the ice surface, as well as the point when all the ice had melted in that part of the tank. The second camera was an infrared camera, which measured the ice surface temperature every 30 minutes.

During the second period of experiments another instrument, the so-called wire harp, was added to measure the bulk salinity in several layers of the ice. A wire harp consists of eight wire pairs with a horizontal spacing of 1 cm between the wires and a vertical spacing of 1 cm (small wire harp) to 2 cm (large wire harp) between the wire pairs (Figure 3.3 (a)). At each wire-pair level, a thermistor is installed to measure the ice temperature. Since the freshwater ice crystals are good insulators, the solid fraction of sea ice can be measured by changes in impedance on the wire pairs. Together with the measured ice temperature the bulk salinity of the sea ice can be calculated. *Notz et al.* (2005) used such wire harps already before and described the functionality in detail. The results from the wire harp measurements of the experiments of the second period of measurements will be discussed in *Jardon et al.* (in preparation).

The setup for the second period of experiments is shown in Figure 3.1 (b), which varies little compared to the setup of the first period. A set of four wire harps (three small ones and a large one) was deployed in the middle of the right part of the tank, next to the ruler. Depending on the ice thickness the wire harps were placed one below the other (very thick ice of up to 26 cm) or next to each other (thinner ice of 10 cm). To test the measurements from the wire harps, some ice cores were taken with an ice drill especially built for the laboratory (Figure 3.3 (b)). The ice drill is a smaller version of the ones used for field work (diameter = 4.7 cm). The amount of ice cores was restricted to the ice area that was still free of instruments and not used for measuring the ice surface temperature with the infrared camera. Therefore, the ice cores were taken in the left part of the tank, even though the ice was thinner there.

The levels at which the three CTDs on the frame were installed changed during the second period again according to different ice thicknesses and water levels. The sensors of the uppermost CTD, the CTD in the upper middle and the CTD in the lower middle were located at 11.5 cm to 35.5 cm, 27.5 cm to 38.5 cm and 65 cm to 79.5 cm water depth, respectively. In addition to the fixed CTDs a moveable CTD (RBR XR-620) was deployed in the middle of the tank. A heating wire was wrapped around the cable in order to unfreeze the cable for lowering the CTD when the ice thickness increases. The objective of adding the moveable CTD was to measure changes in salinity directly underneath the ice. The height of the pumps changed also among the experiments between 24 cm and 40 cm. The large thermistor chain was only used during the experiments with ice thicker than 10 cm. The ice thickness was measured in some experiments with three more rulers. Two were placed at the walls and the third one was added to the first into the middle of the right part of the tank. Moreover, the ventilator was placed next to the right side of the tank to allow for a better mixing of the air, since slightly lower air temperatures were observed at the right side of the tank which might have been the reason for the thicker ice there. Nevertheless, the ice still grew thicker in that part of the tank. The infrared camera pictures were taken every 15 minutes during the last two experiments.

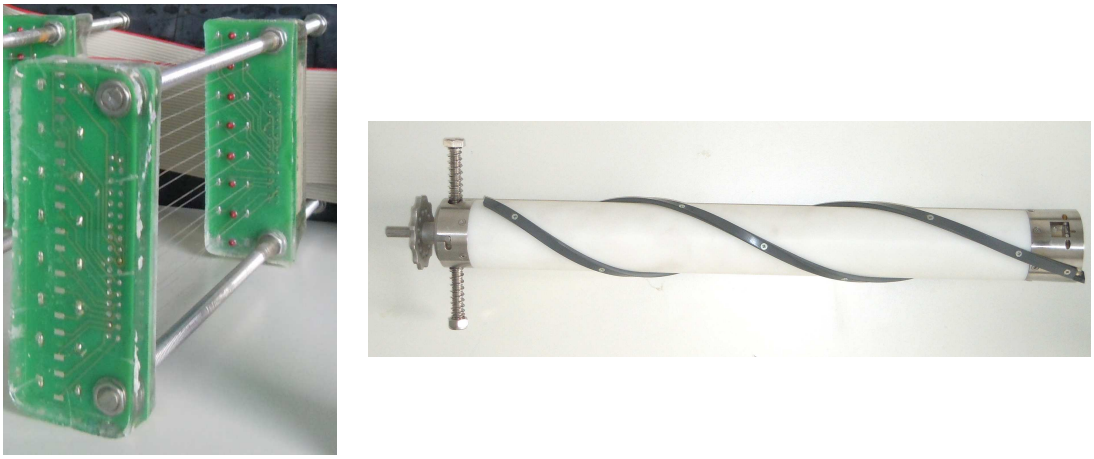

(a) (b)

Figure 3.3: *Small wire harp (a) and laboratory ice drill (b).*

3.2 Experimental setup

The experiments were performed under different conditions. The water salinity, air temperature, oceanic heat flux, duration of ice growth and thus the resulting ice thickness could be varied. Furthermore, the pumps could be turned on. Before starting an experiment, the water was well mixed with the pumps and cooled down close to the freezing point according to the salinity of the water.

During the first period of measurements, the ice was always grown at -20°C air temperature for roughly 40 hours until an ice thickness of around 10 cm was reached. Then melting was initiated by setting the air temperature to a value above 0°C. In Table 3.1 the conditions under which the melting took place during the different experiments are listed. Since Experiment 1 and 2 were just test experiments, they are not included. At the end of the second period of measurements another experiment was conducted in the same way as Experiment 3. Therefore, this experiment is listed in Table 3.1 as well.

The beginning of an experiment is defined as the time when the first ice crystals formed at the water surface which could be observed with the webcam. The point in time when all the ice was melted inside the tank was taken as the end of an experiment. Those times are also listed in Table 3.1.

During most of the experiments, the salinity was chosen to have a value typical of

Table 3.1: *Overview of the experiments of the first period of measurements. Exp.: Experiment, S: initial water salinity, T_{sam}: set air temperature for melting, Q_w: oceanic heat flux.*

Exp.	Duration of ice growth [h]	Duration of ice melting [h]	S [g kg^{-1}]	T_{sam} [°C]	Q_w [W m^{-2}]	Pumps
3	44	79	0	10	15	off
4	36	63	12.7	10	15	off
5	42	68	28.7	10	15	off
6	42	19	28.6	10	15	on
7	41	38	28.7	10	0	on
8	42	36	28.6	15	15	on
9	41	55	28.6	10	15	shortly on
10	44	128	28.3	5	15	off
11	42	63	28.4	10	15	shortly on
18	44	85	0	10	15	off

the surface water in the Arctic Ocean. In Experiment 4 the salinity was approximately half of that value, which could represent for example sea ice in parts of the Baltic Sea. During that experiment the ice was partly flooded with water during melting since it was pushed down by instruments. Furthermore, two freshwater ice experiments (Experiment 3 and 18) were performed to find out more about how the salt within sea ice influences the melting.

The air temperature was set to values between 5 and 15°C. Such high temperatures are rather unusual above sea ice in the Arctic, but nevertheless these temperatures were chosen to have the possibility to perform several experiments during a little less than two months. A whole experiment (including the cooling of the water before starting the ice growth) lasted approximately one week. Inside the cold room, shortwave radiation was not present, which plays an important role in summer sea-ice melting in the Arctic. Conditions similar to those of the laboratory can occur during the polar night in the Arctic.

The oceanic heat flux was set to 15 W m^{-2}, except for Experiment 7, in which the heating wire which generates the oceanic heat flux was turned off. Although the oceanic heat flux in the Arctic Ocean is rather 2 W m^{-2} (*Wadhams,* 2000), the 15 W m^{-2} were chosen in order to avoid supercooling of the water. Supercooled water could result in ice growth around everything that is in the water, like for example the CTDs.

During Experiments 6 to 8, the pumps were continuously turned on during melting in order to avoid a stratification of the water due to the meltwater at the top and to be able to calculate the bulk salinity of the ice out of salt mass conservation in the tank. During ice growth the pumps are not needed since salt loss of the ice leads to convection in the water so that the water is well mixed. The ice melted very fast with the pumps turned on during melting and thus not many ice thickness measurements could be done. Hence, the pumps were turned on only roughly 10 minutes before each ice thickness measurement during Experiment 9 and 11.

During the second period of measurements, the ice was grown at -20°C to -25°C air temperature until an ice thickness of 10 to 26 cm was reached. When the desired ice thickness was obtained, the air temperature was increased stepwise in order to warm the ice slowly and let the ice become permeable. The number of steps and chosen air temperatures varied between experiments. The oceanic heat flux was mainly set to 15 W m^{-2}. During the last experiment, the oceanic heat flux was changed several times to lower or higher values. During all these experiments, the salinity of the water was 33 g kg^{-1}. The pumps were turned off during the first three experiments. For the last three experiments the pumps were turned on both during ice growth and melting. Table 3.2 gives an overview of the experiments of the second period of measurements. The variations of the oceanic heat flux are not listed there, since these are not important for the further analysis of these experiments in the course of this thesis.

During the second period, several things did not work as planned. In Experiment 12, the uppermost CTD was installed closer to the ice bottom to get salinity measurements directly underneath the ice. As a result, the ice grew around the upper part of the CTD and was not free floating during most of the melting time. Hence, the ice was partly flooded with water. In Experiment 13 the ventilator was not turned on until several hours after the melting started, which enabled cold air to stay inside the tank which caused very slow melting at the beginning. In Experiment 15, the ice was frozen onto the walls of the tank during ice growth and thus the ice was not afloat anymore. Hence, the experiment was terminated earlier by opening the door of the cold room and allowing the ice to melt at room temperature. The next experiment was not more successful since the energy supply for the heating plates around the tank broke so that Experiment 16 had to be terminated after only few hours of ice growth as well.

Table 3.2: *Overview of the experiments of the second period of measurements. Exp.: Experiment, T_{sam}: set air temperature, h: ice thickness, r. t.: room temperature (approximately 20°C) when the door of the cold room was opened.*

Exp.	Duration of experiment [h]	T_{sam} steps [°C]	max. h [cm]
12	130	after 40 h, → -15°C after 46 h, → -10°C after 52 h, → -5°C after 63 h, → -2°C after 69 h, → 0°C after 72 h, → 10°C after 118 h, → r. t.	11.6
13	103	after 40 h, → -15°C after 46 h, → -10°C after 52 h, → -5°C after 61 h, → -2°C after 64 h, → 0°C after 71 h, → 10°C	10.8
14	285	after 85 h, → -10°C after 139 h, → -3°C after 158 h, → 0°C after 180 h, → 4°C after 228 h, → 15°C	18.5
15	159	after 127 h, → r. t.	18.9
16	66	after 21 h, → 7°C after 49 h, → r. t.	5.4
17	714	after 246 h, → -13°C after 296 h, → -7°C after 323 h, → -3°C after 343 h, → -10°C after 360 h, → -20°C after 393 h, → -10°C after 455 h, → -2°C after 506 h, → 5°C after 526 h, → -20°C after 558 h, → -7°C after 601 h, → -3°C after 647 h, → 0°C after 670 h, → 5°C after 694 h, → 10°C	26.0

3.3 Instruments and Calibration

3.3.1 Thermistor chains

The resistance of the thermistors changes with temperature. It increases with a decreasing temperature. The relation between resistance and temperature can be calculated with the Steinhart-Hart equation:

$$T = \frac{1}{a + b\ln R + c(\ln R)^2 + d(\ln R)^3} \tag{3.1}$$

T corresponds to the calculated temperature of the measured resistance R.

In the datasheet of the thermistors a table of resistance and respective temperature values is given. These values are assumed to be right for one of the thermistors, which was chosen as the reference thermistor for a calibration before inserting the thermistors into the chains. Out of the values from the datasheet, the coefficients for Equation 3.1 were calculated for the reference thermistor. All thermistors were placed together with the reference thermistor into alcohol that was cooled at different temperatures. The temperature was measured with the reference thermistor and a table of the respective resistance of the other thermistors was created out of which the coefficients for Equation 3.1 were calculated with a polynomial fit for each thermistor. The measuring accuracy of the used thermistors is $\pm$ 0.2 °C for temperatures between 0 °C and 70 °C.

Despite of this calibration, the measured temperatures still varied by some tenth of °C between thermistors. To remove these variations, the thermistor chains were deployed horizontally in the tank at the same height as one of the CTDs, which has a very accurate temperature sensor. The air and water temperature was set to 2 °C and the water was well mixed with pumps. The temperature was measured every 10 seconds by the thermistor chains and the CTD for five hours. For each thermistor the deviation from the CTD was calculated for each measurement. The mean deviation over the five hours (between 0.01 °C and 1.22 °C) was subtracted from the temperature measured by the thermistors during the experiments.

3.3.2 Infrared camera

The infrared camera used for the experiments was a 'VarioCAM high resolution' from InfraTec. It measures longwave radiation between 7.5 and 14 µm. The obtained picture

has 384 x 288 pixel. The measuring range is between -40 °C and 1200 °C with a temperature resolution of 0.1 K. The measuring accuracy is $\pm$ 1.5 K for temperatures between 0 °C and 100 °C and $\pm$ 2 K for temperatures below 0 °C (*InfraTec*, 2007).

Since the last calibration of the camera was done in 2007, a new calibration was conducted at temperatures relevant for the experiments. Therefore, the water inside the tank was cooled down to 2.5 °C and 0 °C and well mixed with the pumps. The air temperature inside the cold room was set to the same temperature. It was assumed that the water temperature at the surface was the same as the temperature deeper in the water due to the mixing. Thus, one of the CTDs was chosen to measure the reference temperature, since the temperature sensor of the CTD is very accurate. The infrared camera was directed towards the water surface and measured the brightness temperatures of the water surface under the assumption of an infrared emissivity of 1.

The temperatures measured by the infrared camera were between 0.8 °C and 1 °C higher than the temperatures measured by the CTD. Since the difference between the water temperatures at which the calibration measurements were done is rather small, a linear regression of the deviation for higher or lower temperatures was not applied. Moreover, the deviation was already measured at relevant temperatures. Hence, just an offset of 1 °C was subtracted from the measured brightness temperatures. This subtracted offset includes already an emissivity correction. In fact, the infrared emissivity for water and ice is a bit lower than 1. The emissivity of water is 0.993 (*Buettner and Kern*, 1965). *De La Rosa et al.* (2011) measured a mean emissivity of 0.9968 for frazil and pancake ice during tank experiments. Even a correction for lower emissivities like 0.97 as *Eisen and Kottmeier* (2000) proposed for sea ice, would lie in the range of accuracy of the infrared camera and can thus be neglected with the assumption of water and sea ice having approximately the same infrared emissivity.

Chapter 4

Results

In this chapter the results from the laboratory experiments are presented. Additionally, model studies are done. Throughout the whole chapter sea ice is compared to freshwater ice in order to clarify the effect of salt within sea ice. How fast ice melts under different conditions is presented in Section 4.1. In Section 4.2 detailed temperature profiles are shown. Finally, in Section 4.3 the ice surface temperature under different conditions is analysed. Even though this thesis focuses on melting sea ice, in some sections the sea-ice growth will be analysed as well, since the data is available from the 'ice growth part' of the experiments and it is worth showing them.

4.1 Melt rate

This section deals with the speed at which the ice thickness decreases. At first, ice thickness measurements from some selected experiments of the first period of measurements are presented in Section 4.1.1. In this context, the dependency of the ice thickness and melt rate evolution on the initial salinity of the water the ice was grown out of is analysed. The measurements are compared with the results of a numerical model that is used for further studies in section 4.1.2. Furthermore, the dependency of the melt rate

on the initial water salinity is investigated in more detail. Additionally, the melt rate of freshwater ice and sea ice as a function of the atmospheric and oceanic heat flux will be analysed by means of the model.

4.1.1 Measurements

The ice thickness h was measured at a ruler frozen into the ice in the middle of the right hand side of the tank (Figure 3.1 (a)). The ice did not grow homogeneous all over the tank. Since the ice was a bit thicker on the right hand side of the tank, the measurements mainly took place in that part of the tank. Additionally, the ice was thinner close to the walls due to the heating plates. When the ice reached a thickness of 10 cm in the middle of the tank, the ice was roughly 2.5 cm thinner at the walls.

Figure 4.1 shows the evolution of the ice thickness in different experiments of the first period of measurements after the air temperature was changed to +10 °C inside the cold room. The initial water salinity S varies from 0 g kg^{-1} to 28 g kg^{-1}. In some experiments pumps were turned on during the whole experiment or shortly before the ice thickness measurement was done to mix the water. During the night no thickness measurements were done, which causes some gaps in the data. The temperature was changed to melting conditions primarily in the morning so that the ice thickness measurements could be done during the air temperature change and during the first hours of melting. Towards the end of the experiments the ice became less homogenous, so that it became more difficult to read a representative ice thickness at the ruler. Therefore, no more thickness measurements were done during the last hours of the experiments. The point of time, when the ice was melted completely, could be determined with the aid of the webcam and the infrared camera. This moment is taken as the last ice thickness measurement.

The measurements show that independent of the initial water salinity, the ice still grows for a short period of time after the temperature is changed to melting conditions. However, the melt duration varies among the different experiments (Figure 4.1). Sea ice melts faster than freshwater ice. Moreover, when pumps were turned on all the time during melting, sea ice grown out of water with the same salinity melts faster. This faster melting might be affected from turbulence underneath the ice caused by the pumps, which could increase the oceanic heat flux. This effect might be enhanced by the uneven ice bottom during melting which causes locally larger horizontal temperature gradients than at an even ice bottom.

In order to investigate the influence of salt on the melting process in greater detail, ex-

periments with different initial water salinities that were performed under nearly equal conditions (Exp. 3, 4, 5, 9 and 18) are compared. In the chosen five experiments, ice was grown at -20 °C air temperature over roughly 42 hours. The maximum ice thickness reached 10.2 cm to 11.1 cm. The air temperature was set to +10 °C during melting. The pumps were turned off during the whole experiment, except for Experiment 9. In that experiment the pumps were turned on ten minutes before each ice thickness measurement during melting in order to obtain relatively well mixed water without increasing the melting. Without mixing, a warmer freshwater layer could develop out of meltwater directly underneath the ice bottom. In fact, the water temperature underneath the ice was approximately 0.4 °C higher than the freezing temperature during those experiments. This freshwater layer could effect the melting by reducing heat and salt exchange with the underlying water. The chosen experiments include two freshwater experiments (Exp. 3 and 18) and three seawater experiments with salinities of 12 g kg^{-1} and 28 g kg^{-1}.

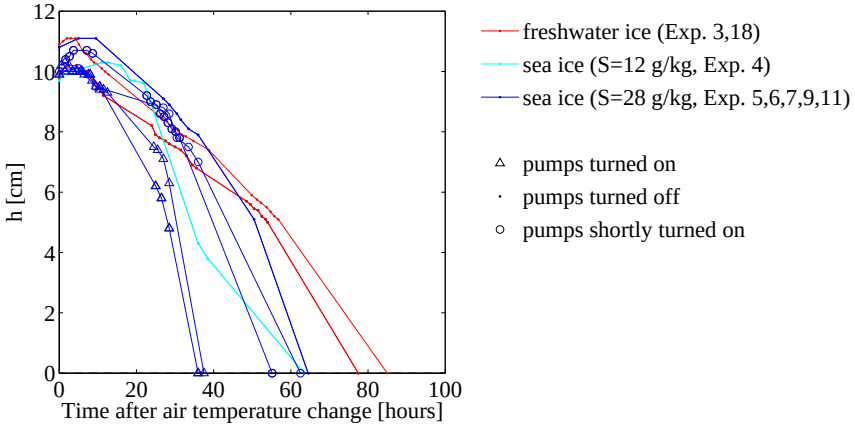

Figure 4.1: *Measured temporal evolution of the ice thickness h during melting. Each dot, triangle or circle marks one measurement. S corresponds to the initial water salinity, i.e. the salinity of the water shortly before the ice growth started.*

Figure 4.2 (a) shows the measured ice thickness h of the chosen experiments and Figure 4.2 (b) shows the melt rate, which is the change of ice thickness per unit time. The melt rate is calculated from one-hourly values that were obtained by linear interpolation. A running mean with a window of eight hours is applied to the interpolated data in order to smooth the data. The melt rate shows that at first, freshwater ice melts faster than sea ice, but after roughly 17 hours sea ice melts faster. The melt rate stays relatively constant at 0.1 cm h^{-1} for freshwater ice, while it increases over time for sea ice, until reaching a maximum of around 0.35 cm h^{-1} towards the end of the experiments. In the beginning of the melting process in Experiment 4, the ice melts much more slowly than during the

other experiments. On the other hand, after some hours the melt rate increases suddenly very fast and the maximum is reached earlier than during the other experiments with seawater. The reason might be that the ice was partly flooded with water during the first 18 hours, which prevented the ice from a direct contact with the warm air. All in all, sea ice of the same thickness melts faster than freshwater ice.

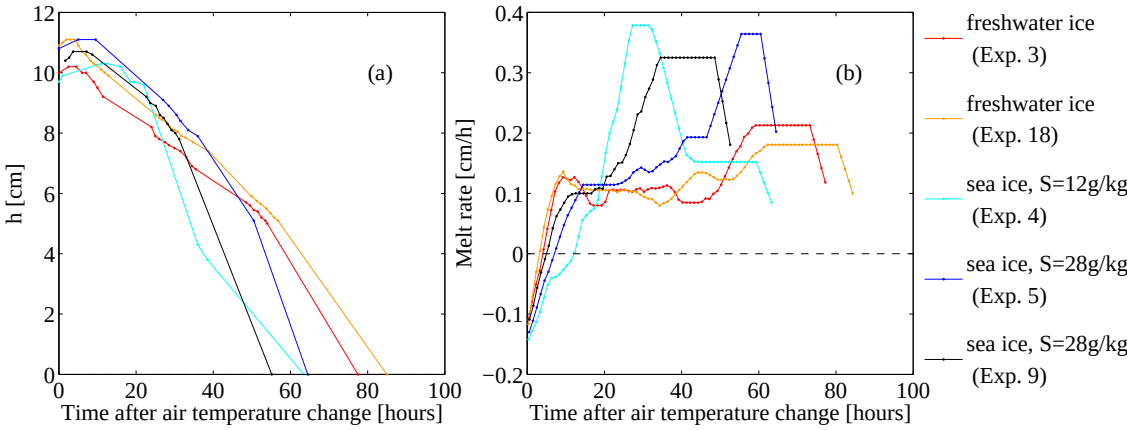

Figure 4.2: *Measured temporal evolution of the ice thickness h during melting (a) and melt rates (b) in Experiments 3, 4, 5, 9 and 18. Each dot in (a) marks one ice-thickness measurement. S corresponds to the initial water salinity.*

The delayed start of sea-ice melting can be explained by the longer time needed to warm sea ice compared to freshwater ice. More time is needed since more energy is needed to warm the ice. This is due to internal melting which occurs as the ice temperature rises. Higher ice temperatures require lower brine salinities to keep thermal equilibrium, which can only be obtained by partly melting the freshwater-ice crystals. This additionally needed energy for warming sea ice is included in the heat capacity of sea ice (Figure 2.2 (a)). On the other hand, as sea ice gets warmer, it also becomes more porous since the solid fraction decreases due to the internal melting. Hence, it requires less energy to melt sea ice after warming it than freshwater ice. This is described in the latent heat of fusion which gets smaller with increasing bulk salinity and increasing temperature (Figure 2.2 (c)). Therefore, the melt rate of sea ice increases with time because the remaining latent heat decreases as the temperature increases. The impact of surface and bottom melting is discussed in Section 4.2.

4.1.2 Model

For further analysis of the melt rate, the thermodynamic sea-ice model SAMSIM developed by *Griewank and Notz* (submitted) is used. It is a multi-phase 1D model, in which vertical desalination processes like gravity drainage and flushing are included through parametrisations. The model is based on the mushy-layer equations of sea ice (*Feltham et al.*, 2006). It has a variable number of layers with varying thickness depending on the ice thickness. In each layer the enthalpy, absolute salinity, mass and thickness are given and other quantities such as the ice temperature are derived from them with the assumption of thermal equilibrium. The lowest layer represents the ice-ocean-interface. In that layer the solid volume fraction always lies beneath a certain value. When it becomes higher, a new layer of ice forms.

In the model setup used here the atmospheric heat flux Q_a at the ice surface is assumed to be a linear function of the temperature difference between the air temperature T_a and the ice-surface temperature T_s:

$$Q_a = C(T_a - T_s) \tag{4.1}$$

C corresponds to the heat transfer coefficient. For melting, C is reduced by a reduction parameter RP to reflect the smaller heat exchange in the stable stratified air above the ice, which evolves due to the ice surface temperature being lower than the air temperature. A more precise model description can be found in *Griewank and Notz* (submitted).

As a first step the model is tested to see whether it can reproduce the laboratory measurements, which is done for the five experiments that were analysed in Figure 4.2 in the previous section. The oceanic heat flux, the water salinity, the air temperatures during ice growth and melting, and the time of ice growth are set to measured values. The heat transfer coefficient and the reduction parameter are adjusted in the model for these experiments. These parameters and their values are summarized in Table 4.1. The oceanic heat flux is not listed in Table 4.1 since it was 15 W m^{-2} during all experiments. The values for the heat transfer coefficient and reduction parameter were found by trying to reproduce the shape of the ice thickness evolution with realistic values. *Naumann* (2011) calculated the heat transfer coefficient during experiments within the same tank inside the same cold room as used for these experiments. The calculations resulted in values between 14.8 and 27.1 W m^{-2} °C^{-1}. In the model the heat transfer coefficient is mostly set to values below the calculated values from *Naumann* (2011). The air temperature in the model is changed by one-hourly steps according to the measured air temperatures until the mean melt air temperature is reached. For example, inside the cold room, it takes roughly four hours for a temperature change from -20 °C to 0 °C. Before calculating the

Table 4.1: *Values for water salinity S, time of ice growth t, air temperature during ice growth T_{ag}, air temperature during melting T_{am}, the heat transfer coefficient C and the reduction parameter RP for the modelled laboratory experiments. The oceanic heat flux was set to 15 W m^{-2} in all experiments.*

Exp.	S [g kg^{-1}]	t [h]	T_{ag} [°C]	T_{am} [°C]	C [W m^{-2} °C^{-1}]	RP
3	0	43.75	-17.5	7.7	16	1.5
4	12.7	35.7	-19.4	7.9	13.5	1.0
5	28.7	43.5	-19.5	7.9	13.2	1.3
9	28.6	31.7	-19.4	7.7	12.5	1.1
18	0	43.65	-19.0	8.2	16.5	1.5
6	28.6	42.25	-19.3	7.8	12.5	1.3
7	28.7	40.5	-19.0	7.2	14	1.3

melt rate from the modelled ice-thickness data, a central running mean with a window of eight hours is applied to the data, as it is done for the measured ice thickness in the previous section.

A comparison of Figure 4.2 and Figure 4.3 shows that measurement and model results agree quite well. The general structure of the ice thickness and melt rate evolution is reproduced by the model. The main difference is that in the model more time is needed until the ice melted completely, independent of salinity. On the one hand, the maximum ice thickness is the same as in the measurements. But on the other hand, at the point of air temperature change the ice is thinner in the model and it reaches the maximum thickness around three hours later than in the laboratory experiments. As a result, the ice thickness decrease started later in the model than in the laboratory experiments, which might partly cause the delay in the complete ice melting of around ten hours. Furthermore, there is a more distinct gap in the melting start between freshwater ice and sea ice in the model. In the laboratory experiments the thickness decrease started only two hours later for sea ice than for freshwater ice. For sea ice it takes around ten hours before the ice thickness starts to decrease and for freshwater ice it takes roughly five hours. The melt rate is constant at around 0.1 cm h^{-1} for freshwater ice like in the measurements. The sea-ice experiments show an increase in the melt rate up to maximum values between 0.27 and 0.37 cm h^{-1}. After reaching the maximum melt rate, it decreases again. The maximum melt rate is approximately the same in the modelled Experiments 4 and 9, but much lower for Experiment 5. Interestingly, the melt rate of the modelled Exper-

iment 4 shows a similar sudden strong increase after 20 hours as in the measurements. This similar increase could be a sign that the flooding of the ice during Experiment 4 did not have a great influence. More similar experiments should be conducted to investigate this interesting observation in more detail, which was not possible during the limited time for this study.

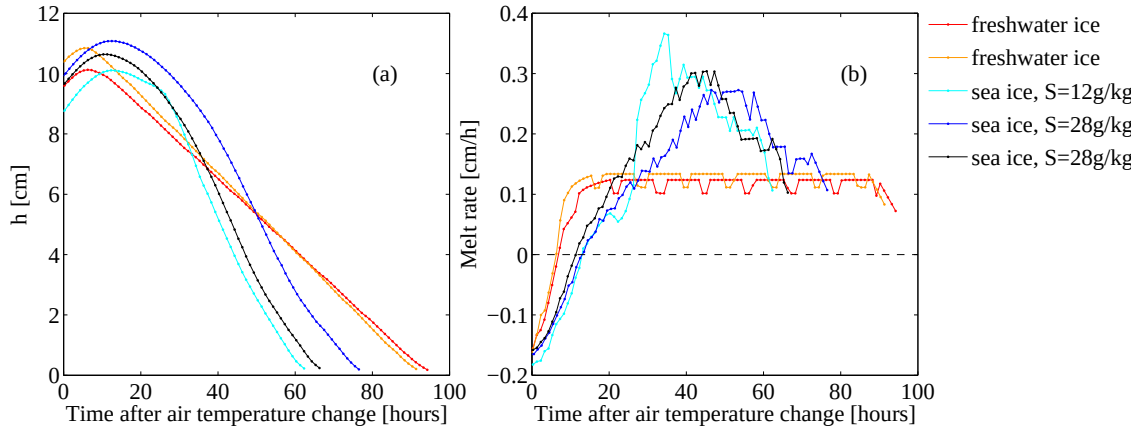

Figure 4.3: *Modelled temporal evolution of the ice thickness h during melting (a) and the melt rate (b) in Experiments 3, 4, 5, 9 and 18. S corresponds to the initial water salinity.*

The dependency of the melt rate on the initial water salinity is analysed in more detail by means of the model. Further, a dependency of the melt rate on the atmospheric and oceanic heat flux is investigated. Therefore, a reference model experiment is set up, from which different parameters are changed for the different analyses. The parameters of this reference experiment are chosen to be similar to the five analysed laboratory experiments, since these can be reproduced well by the model. In Table 4.2 the parameters and values of the reference experiment are shown. The air temperature is changed in 14 one-hourly steps from T_{ag} to T_{am}. The analysis on the atmospheric and oceanic heat flux dependency is done for both freshwater ice and sea ice.

For the analysis on the salinity dependency of the melt rate, eight different water salinities between 0 and 30 g kg^{-1} are chosen. Figure 4.4 shows how the ice thickness and melt rate vary with water salinity. Freshwater ice melts at a constant rate of 0.13 cm h^{-1} from around 15 hours onwards while the melt rate shows a distinct maximum for sea ice. Ice grown out of water with a salinity between 15 and 30 g kg^{-1} shows nearly the same melting behavior. The melt rate increases for 40 hours until it reaches a maximum of nearly 0.3 cm h^{-1}. Afterwards, the melt rate decreases again. For water salinities of 5 or 10 g kg^{-1}, the melt rate increases more slowly, but after 35 hours a strong increase up to a maximum of nearly 0.4 cm h^{-1} occurs. Thereafter, the melt rate behaves similar to sea ice

Table 4.2: *Setup of the reference model experiment. Q_w: oceanic heat flux, t: time of ice growth, T_{ag}: air temperature during ice growth, T_{am}: air temperature during melting, C: heat transfer coefficient, S: water salinity, RP: reduction parameter.*

Parameter	Value
Q_w	15 W m^{-2}
t	42 h
T_{ag}	-19.5 °C
T_{am}	8.0 °C
C	13.5 W m^{-2} °C^{-1}
S	0 g kg^{-1} resp. 30 g kg^{-1}
RP	1.2

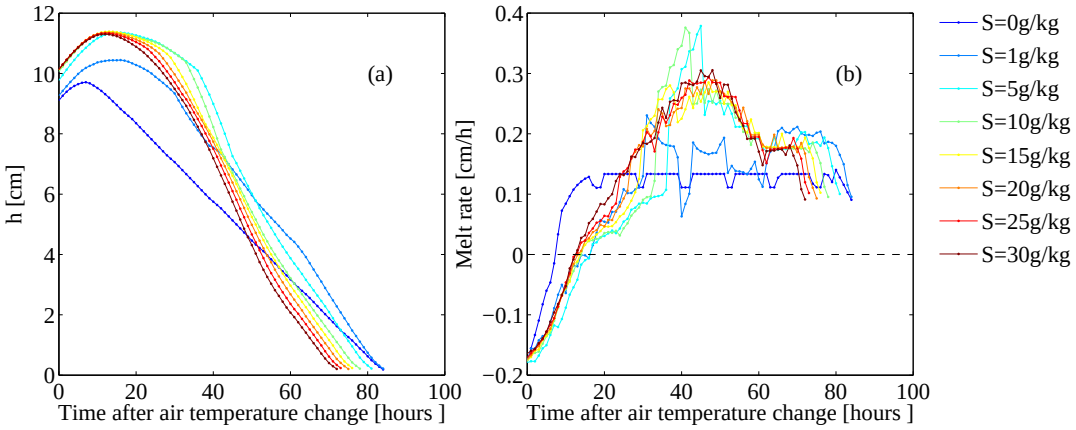

Figure 4.4: *Modelled temporal evolution of the ice thickness h during melting (a) and melt rate (b) as a function of the initial water salinity S.*

with higher salinities. The melt rate of sea ice grown out of water with a very low salinity of 1 g kg^{-1} jumps between 0.2 and 0.1 cm h^{-1}. Even though this sea ice is very close to freshwater ice, the ice thickness decrease starts around 5 hours later than for freshwater ice as it does for sea ice with higher salinities. All in all, sea ice grown out of water with a salinity higher than 1 g kg^{-1} melts faster than freshwater ice.

In the model the atmospheric heat flux is changed by changing the heat transfer coefficient. With Equation 4.1, different heat transfer coefficients C could be trans-

formed into variations of the atmospheric heat flux Q_a. The air temperature T_a does not change between experiments. Assuming the ice surface temperature T_s not to change as well, the atmospheric heat flux increases linearly with an increasing heat transfer coefficient C. For the analysis on the atmospheric heat flux dependency of the melt rate, the heat transfer coefficient is changed by equidistant steps of $5\,\mathrm{W\,m^{-2}\,{}^{\circ}C^{-1}}$ between 5 and $25\,\mathrm{W\,m^{-2}\,{}^{\circ}C^{-1}}$. Figure 4.5 shows the results for the freshwater-ice experiments. In Figure 4.6 the sea-ice experiments are presented. Independent of salinity, ice grows thicker and melts faster at higher atmospheric heat fluxes. The melt rate of freshwater ice is constant after the ice thickness decrease started. This constant value increases proportionally with an increasing heat transfer coefficient. The ice growth is influenced by the ice thickness, since heat has to be conducted through the ice. Since ice is a good thermal insulator, ice growth becomes slower with thicker ice. Hence, the ice grows exponentially. In contrast, the melting does not depend on the thickness since it takes place both at the ice surface and ice bottom. Thus, the freshwater ice melts linearly. As a consequence, the ice exists longest at a certain atmospheric heat flux. This happens in sea ice as well even though the melt rate changes differently. The melt rate has a maximum that occurs earlier with an increasing atmospheric heat flux. This shift might come from a faster warming of the ice at a higher atmospheric heat flux. Thus, the ice gets more liquid faster which simplifies the melting process.

For the analysis of the oceanic heat flux dependency eight different values between $0\,\mathrm{W\,m^{-2}}$ and $30\,\mathrm{W\,m^{-2}}$ were taken for the oceanic heat flux. The higher values can represent the oceanic heat flux in the Antarctic, whereas typical values for the Arctic are around $2\,\mathrm{W\,m^{-2}}$ (*Wadhams*, 2000). In Figure 4.7 and Figure 4.8 the results for the freshwater-ice and the sea-ice experiments are presented, respectively. For both freshwater ice and sea ice around 40 hours more are needed to melt the ice completely with no oceanic heat flux than with the highest value. Freshwater ice grows slightly more than 1 cm thicker with no oceanic heat flux than with the maximum value, whereas sea ice becomes 3 cm thicker. Moreover, the maximum thickness of sea ice is reached later with lower oceanic heat fluxes than with higher, which does not happen with freshwater ice. The melt rate of freshwater ice is constant with time and increases slightly with increasing oceanic heat fluxes. For heat fluxes between $10\,\mathrm{W\,m^{-2}}$ and $30\,\mathrm{W\,m^{-2}}$ the melt rate of sea ice hardly differs. In contrast, the melt rate shows an interesting evolution at lower oceanic heat fluxes and especially when no oceanic heat flux is present. For forty to fifty hours the melt rate is lower than the melt rate at higher heat fluxes. Subsequently, the melt rate suddenly increases up to a maximum of $0.6\,\mathrm{cm\,h^{-1}}$. This strong increase might happen due to the formation of a false bottom on the modelled ice. Freshwater can run off the ice edges and refreeze at the bottom of the ice when the oceanic heat flux is rather small. Hence, the ice still becomes thicker at the bottom for some hours after

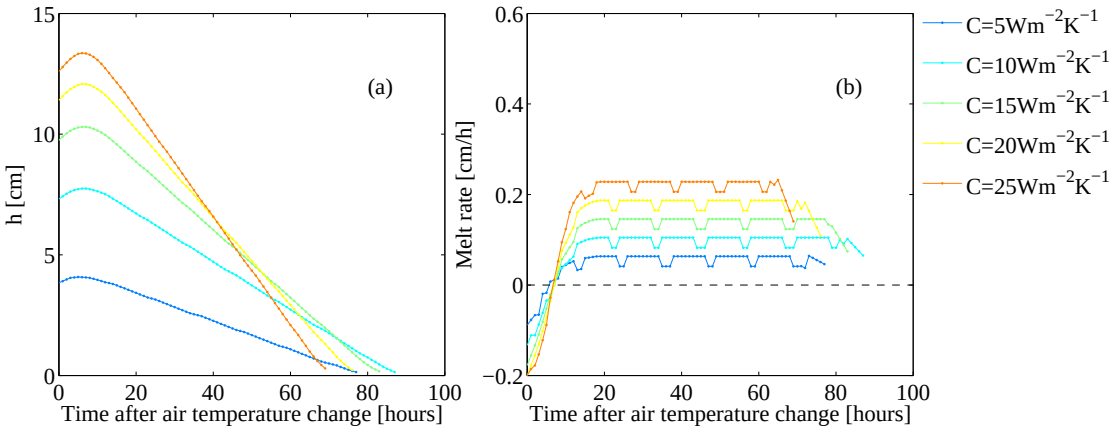

Figure 4.5: *Modelled temporal evolution of the ice thickness h during melting (a) and melt rate (b) of freshwater ice as a function of the heat transfer coefficient C.*

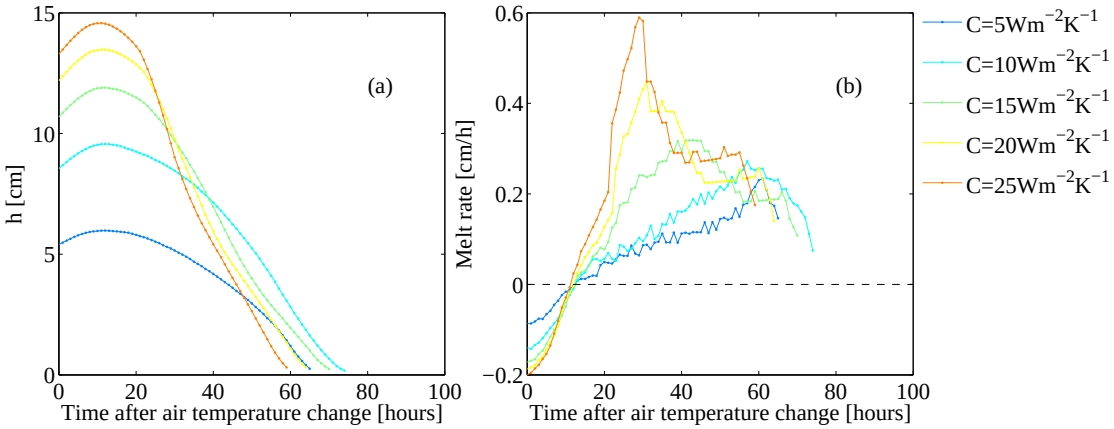

Figure 4.6: *Modelled temporal evolution of the ice thickness h during melting (a) and melt rate (b) of sea ice as a function of the heat transfer coefficient C.*

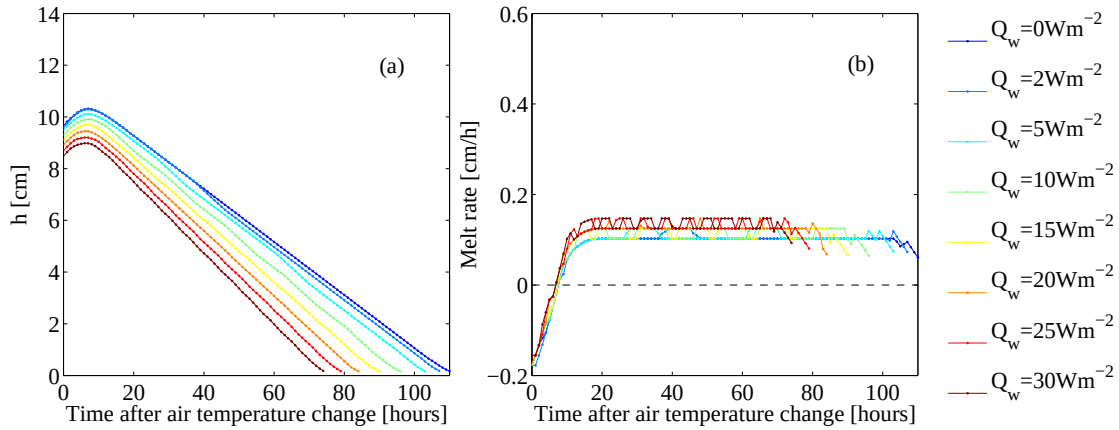

Figure 4.7: *Modelled temporal evolution of the ice thickness h during melting (a) and melt rate (b) of freshwater ice as a function of the oceanic heat flux Q_w.*

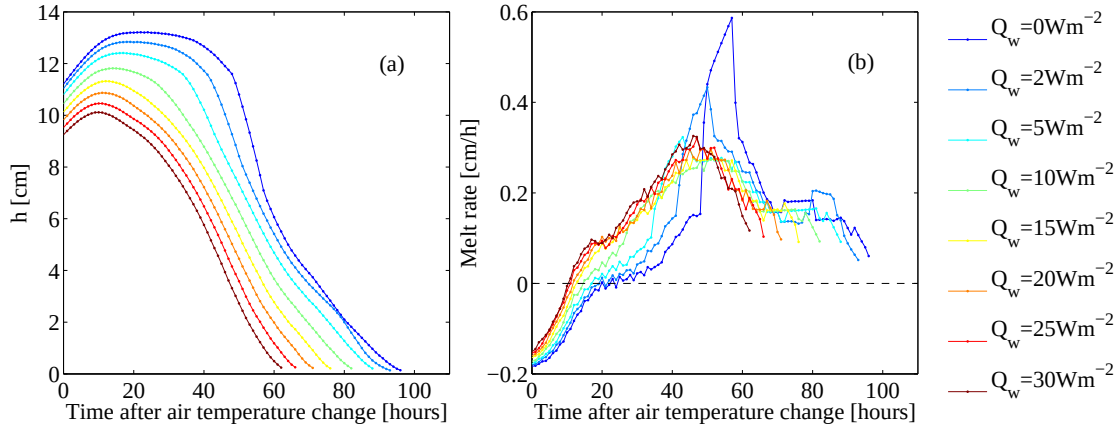

Figure 4.8: *Modelled temporal evolution of the ice thickness h during melting (a) and melt rate (b) of sea ice as a function of the oceanic heat flux Q_w.*

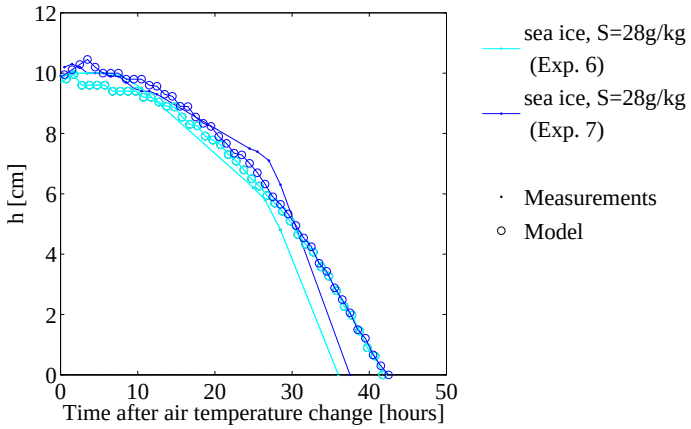

Figure 4.9: *Measured and modelled temporal evolution of the ice thickness h during melting of two experiments with turned on pumps during melting (Exp. 6 and 7).*

switching the air temperature. At the same time the ice warms. At some point, the critical value of the solid fraction in the sea-ice layers above the freshwater-ice layers of the false bottom is exceeded. Then these sea-ice layers are treated as liquid and already melted by the model. Step by step the freshwater-ice layers melt. When the last one of these bottom layers is melted, the ice thickness suddenly decreases by some centimeters, since the layers above the false bottom are already treated as liquid by the model. Therefore, this sudden decrease in sea-ice thickness at lower oceanic heat fluxes is rather a model artefact.

Finally, the influence of the pumps on the evolution of the ice thickness is investigated by means of the model. Figure 4.1 shows that the turned on pumps had a great impact on the evolution of the ice thickness during the laboratory experiments. Turbulence underneath the ice is not included in the model. On the other hand, the additional heat from the heating wire around the pumps and from the pumps themselves can be simulated by increasing the oceanic heat flux in the model. While the oceanic heat flux is kept at $15\,\mathrm{W\,m^{-2}}$ during ice growth, it is increased when the air temperature is changed to melting conditions since the pumps were only turned on during melting. Trying different values resulted in an oceanic heat flux of $100\,\mathrm{W\,m^{-2}}$ to reproduce the ice thickness evolution well. Figure 4.9 shows the measured and modelled ice thickness evolution of two similar experiments with pumps being turned on. The setup of these experiments in the model is listed in Table 4.1. However, an oceanic heat flux of $100\,\mathrm{W\,m^{-2}}$ is higher than the additional heat from the pumps. The power of each pump is only 13.7 W which would result in an increase by $21\,\mathrm{W\,m^{-2}}$. The heating wire around the pumps was only short and its impact is thus rather negligible. This shows that dynamical effects play an important role in the melting process. Warm water can be transport upwards by the pumps, so that the oceanic heat flux increases.

4.2 Internal ice temperature

In this section, the internal ice temperature is analysed in detail. Again, freshwater ice and sea ice are compared. Therefore, one experiment is chosen as an example for each ice type. The results from the laboratory measurements are presented in Section 4.2.1. In Section 4.2.2 the internal ice temperature is further investigated by means of the thermodynamic model which is already used to analyse the melt rate in the previous section.

4.2.1 Measurements

The ice temperature was measured by two thermistor chains. However, here only the data from the short chain is presented since it has the smaller spacing between thermistors and therefore a higher spatial resolution. Moreover, the long thermistor chain was placed at the edge of the ice and its measurements might be influenced by the heating plates around the tank.

For the comparison between freshwater ice and sea ice, Experiment 3 is chosen as an example of freshwater ice and Experiment 5 is taken as an example of sea ice. Both experiments were conducted under the same conditions. 10 cm thick ice was grown and subsequently melted at a constant air temperature of 10°C and a constant oceanic heat flux of 15 $W\,m^{-2}$. The pumps were turned off. Experiment 18 is not selected as freshwater-ice example, because one of the upper thermistors in the small thermistor chain did not work. Experiment 5 is selected from all the sea-ice experiments because during that experiment an interesting temperature evolution was observed which is focused on later in this section.

Figure 4.10 and Figure 4.11 show the ice temperature from Experiment 3 and Experiment 5, respectively. Note that the same colours in both figures do not display the same temperatures. White indicates the respective freezing point of the water the ice was grown out of. However, the interval between colours and temperatures is the same. In addition, the air temperature measured with the temperature sensor above the ice and the ice surface temperature measured with the infrared camera are shown in the upper part of the figures. Even though the air temperature inside the cold room was set to the same values during both experiments both for ice growth and melting, the real air temperature was different between the two experiments. The point of the temperature change to melting conditions is marked by a dashed black line in the figures.

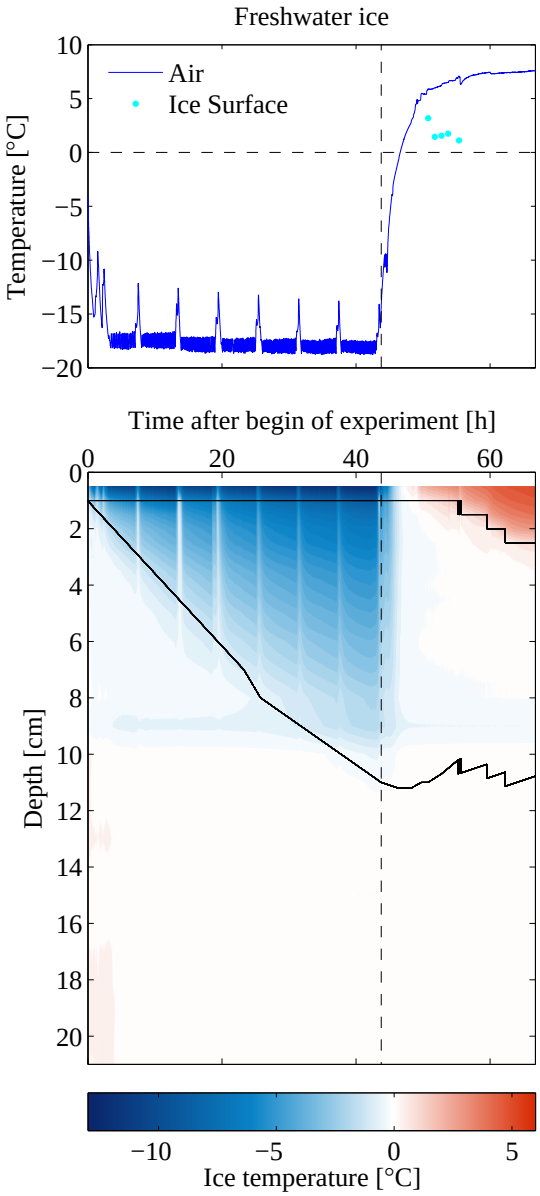

Figure 4.10: *Temporal evolution of the air temperature, ice-surface temperature and internal ice temperature during growth and melting of freshwater ice (Experiment 3). The black solid lines indicate the ice surface and bottom. The black dashed line indicates the time when the air temperature was switched to melting conditions. White areas indicate the freezing point of the water.*

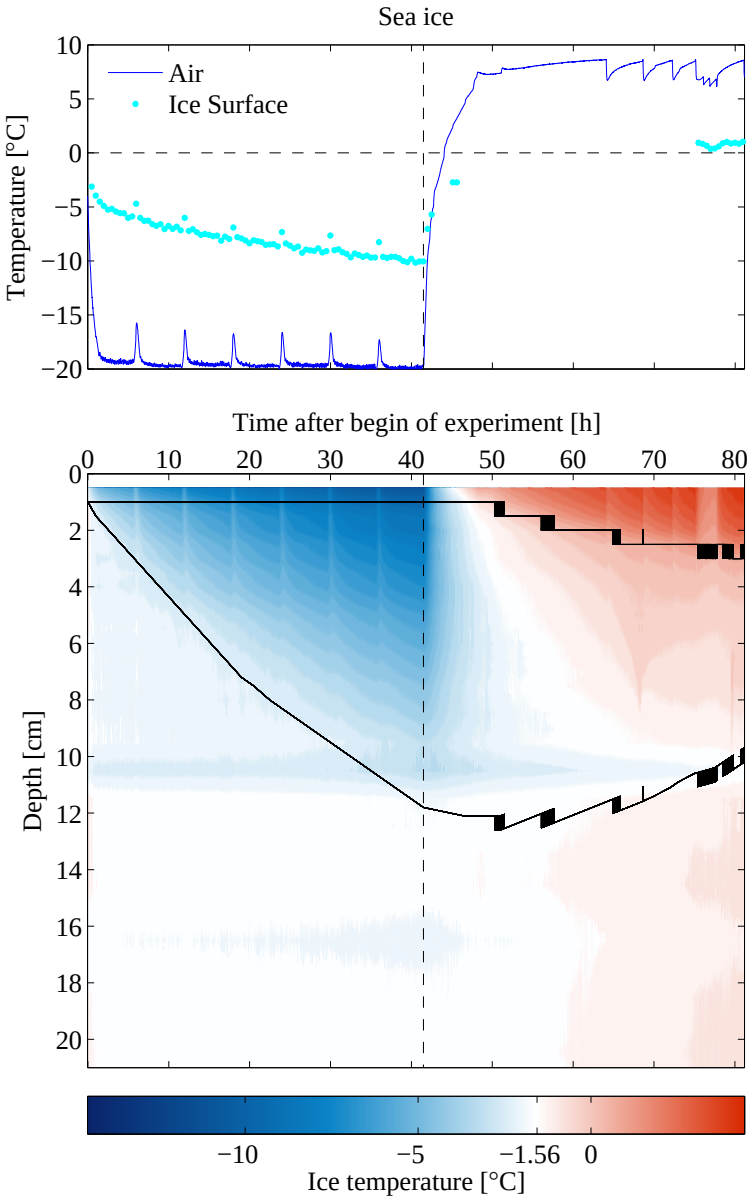

Figure 4.11: *Temporal evolution of the air temperature, ice-surface temperature and internal ice temperature during growth and melting of sea ice (Experiment 5). The black solid lines indicate the ice surface and bottom. The black dashed line indicates the time when the air temperature was switched to melting conditions. White areas indicate the freezing point of the water.*

The temperature measured by the thermistor chain is only shown until the point when the thermistor chain became ice-free. The thermistor chain conducts heat into the ice so that the ice melts slightly faster around the chain. As a result, the chain becomes ice-free at some point and the ice temperature can not be measured until the end of the experiment. The time when the chain becomes ice-free can be determined with the pictures from the webcam. During the melting process the chain moves upwards due to surface melting. When the chain becomes ice-free, this upward movement stops, but the chain can move sideways from then on. Due to turned on pumps and wind from the ventilator, there is always some easy observable movement of the free floating ice and the thermistor chain.

The solid black lines in Figure 4.10 and Figure 4.11 indicate the ice surface and bottom. During ice growth the first thermistor in the ice is taken to indicate the height of the ice surface. Since the spacing of the thermistors is 0.5 cm in the upper part of the thermistor chain, the error is maximum 0.4 cm. Some hours after the temperature is switched to melting conditions, the thermistor chain starts to move upwards due to surface melting and the upper thermistors become ice-free. From then on, the height of the ice surface is determined by the maximum of the temperature gradient. Note that the z-axis is directed from the first thermistor on the chain into the ice. The ice bottom is derived by adding the measured ice thickness to the ice surface height. It can be assumed that the ice thickness is the same both at the ruler and at the thermistor chain since both were deployed close to each other in the tank. In the lines indicating the ice surface and bottom some steps occur. These steps originate from the spatial resolution of the thermistor chain. The bottom line is also influenced by the resolution of the ice thickness measurements on the ruler, which is 0.1 cm.

The depth of the measured ice temperature is given as the distance from the first thermistor. In total, a distance of 21 cm is covered with the short thermistor chain, which includes some air and water temperature measurements besides the ice temperature. The first thermistor does not work so that there exists a gap in the data. Even though the thermistors were calibrated, there is still one thermistor in the middle of the short chain that measured a bit too low temperatures.

During ice growth, in both experiments a linear temperature profile is being established. Furthermore, the ice reacts quickly to the warming of the cold room, which occurs approximately every six hours. This temperature signal is clearly visible in the ice-surface temperature and penetrates into the ice over the whole depth. This warming should be kept in mind whenever laboratory experiments are done in such a cold room, since the warming can for example affect the salinity evolution within the ice. As *Jardon et al.* (in preparation) points out, a warming of sea ice over the whole depth increases the

permeability of the ice and thus makes brine convection possible.

In contrast to ice growth, the temperature evolution during ice melting differs considerably between freshwater ice and sea ice. After the air temperature is switched to a higher value, the freshwater ice warms uniformly over the whole depth and reaches the melting temperature of 0 °C within a few hours (Figure 4.10). Thus, there is no temperature gradient present any more within the ice. Due to surface melting the ice surface lowers continuously, disregarding the steps in the height due to the spatial resolution of the thermistor chain. The ice bottom evolves differently. Comparing the height of the bottom at melting begin with the height when the thermistor chain became ice-free, it barely changes, disregarding the steps due to the resolution of the thermistor chain and the ruler. Thus, the ice melts mainly at the surface, rather than at the bottom of the freshwater ice due to a higher heat flux from the atmosphere than from the ocean.

The temperature evolution in melting sea ice is different. First of all, the ice warms more slowly than freshwater ice since more energy is required due to internal phase changes, as already pointed out in the previous section. Additionally, the warming is not uniform with depth due to variations in bulk salinity within the ice. At the surface and bottom, the ice temperature is at the respective melting point. Thus, the ice temperature is lower at the bottom than at the surface due to a higher bulk salinity at the bottom. A non-linear temperature profile establishes in melting sea ice. This temperature profile allows heat conduction within the ice during melting, which is illustrated in Figure 4.12 in analogy to Figure 2.3. The energy of the atmospheric heat flux Q_a and oceanic heat flux Q_w that is not used for melting, is conducted into the ice. There, the heat further warms the ice. The height of the sea-ice surface decreases more or less continuously, as during the melting of freshwater ice. However, the height of the sea-ice bottom shows stronger changes than the bottom of freshwater ice. The bottom rises over time after the maximum ice thickness is reached. This bottom rise signifies that a stronger bottom melting occurs for sea ice than for freshwater ice. The solid fraction of sea ice decreases with depth so that the ice is already quite liquid at the bottom. Thus, melting sea ice at the bottom does not require as much energy as melting freshwater ice.

During the other sea-ice experiments the general temperature evolution was more or less the same as in Experiment 5. In Experiment 5, an interesting ice-temperature evolution is observable around 25 hours after the air temperature was changed (Figure 4.11). Over a timespan of some hours, the ice temperature increases in the upper two thirds of the ice and decreases again. The temperature reaches up to 0 °C and even slightly more. Such high temperatures can only be measured in freshwater ice and usually not

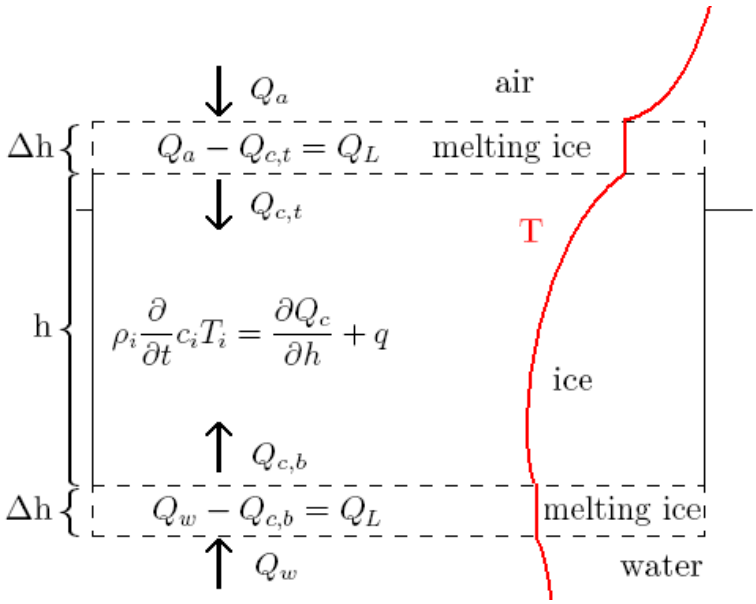

Figure 4.12: *Heat fluxes during ice melting. Q_a: atmospheric heat flux, Q_c: conductive heat flux through the ice, $Q_{c,t}$: conductive heat flux at the top of the ice, $Q_{c,b}$: conductive heat flux at the bottom of the ice, Q_L: latent heat, Q_w: oceanic heat flux, h: ice thickness, Δh: thickness of melting ice, ρ_i: ice density, c_i: heat capacity of the ice, T: temperature, T_i: ice temperature, q: internal heat sources.*

in sea ice, since the melting point of sea ice is lower according to the bulk salinity. The measured temperature increase in Experiment 5 is likely caused by freshwater penetrating through the ice, which is called flushing. The required freshwater comes from the ice surface and consists of meltwater from snow and/or the ice. In the laboratory experiments there was no snow present, so that the meltwater originated only from melted ice. One should keep in mind that the thermistor chain sticking in the ice could have supported or even induced this flushing due to additional heat conduction which let the ice around the chain melt. After the flushing occurred, the ice cools again, because flushing is a local event. Around this area, the sea ice still has lower temperatures due to the non-zero bulk salinity. Hence, the percolated freshwater refreezes inside the sea ice. The refrozen freshwater can build an impermeable freshwater-ice layer, which is of great importance for further brine movement within the ice. Since horizontal gradients are not taken into account in 1D sea-ice models, such an observed flushing event can not be simulated in such models.

In both Experiments 3 and 5 the temperatures measured in the first millimeters of the ice were higher than the respective melting point of the ice. The reason might be meltwater around the thermistor chain. Since the ice melts around the chain, the upper

thermistors are probably in contact with warm meltwater rather than with ice. Measurements of the ice surface temperature are rather sparse for those two experiments. The infrared camera was first installed inside the cold room when the melting during Experiment 3 started. During Experiment 5, the infrared camera stopped recording pictures for unknown reasons. But nevertheless, the few measurements show unexpected high surface temperatures during melting, partly even above 0°C. Therefore, the measured ice-surface temperature will be analysed in more detail in Section 4.3.

4.2.2 Model

In the previous section, Experiment 3 and 5 were chosen as examples for freshwater ice and sea ice to analyse the internal ice temperature. Hence, those two experiments are simulated with the model for the comparison between the model and the measurements. Figures 4.13 and 4.14 show the modelled temperatures of Experiment 3 and 5, respectively. For an easy comparison with the laboratory measurements, the figures are constructed in the same way as those in the previous section. The same colour range is used with white indicating the respective freezing point of the water. The depth is calculated as if the data were measured with the thermistor chain. The model data contains only the ice temperature, but no air temperature directly above the ice or water temperature. A great advantage of the model is that information about the ice temperature is available until the end of the experiment. Thus, two black dashed lines exist in the Figures 4.13 and 4.14. One indicates the time when the air temperature was switched to melting conditions and the other one indicates the time when the thermistor chain became ice-free during the laboratory experiments. In the upper part of the figures, the set air temperature and the ice-surface temperature are also shown.

The evolution of the ice temperature in the model is very similar to the measurements. During ice growth the modelled ice temperature also shows a linear profile in both experiments. The warming of the ice starts slightly later due to the discontinuous air temperature change in the model. Nevertheless, the ice temperature evolution during melting is also similar to the laboratory measurements.

After the air temperature is set to higher values, the freshwater ice warms uniformly until reaching the melting point over the whole depth like in the laboratory experiments. The modelled height of the ice surface shows very well the continuous lowering due to surface melting, which proceeds until the end of the experiment. However, the surface melting started later during the laboratory experiment, which could come from the resolution of the thermistor chain. The modelled height of the ice bottom changes less than the modelled height of the ice surface, like in the measurements.

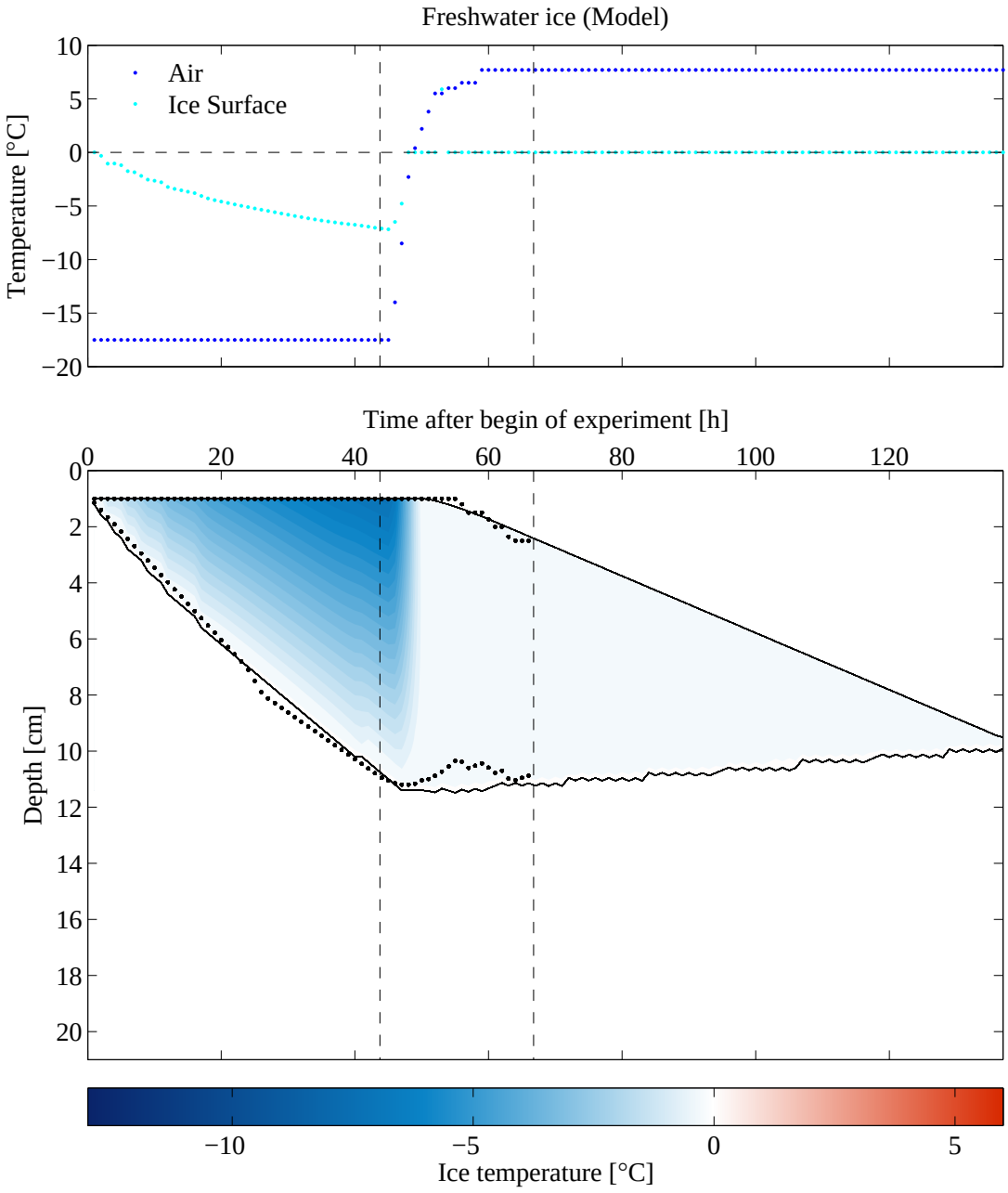

Figure 4.13: *Temporal evolution of the air temperature, ice-surface temperature and internal ice temperature during growth and melting of freshwater ice (modelled Experiment 3). The black solid lines indicate the modelled ice surface and bottom. The black dotted lines indicate an hourly mean of the measured ice surface and bottom. The first black dashed line indicates the time when the air temperature was switched. The second black dashed line indicates the time when the themistor chain in the laboratory experiment became ice-free. White areas indicate the freezing point of the water.*

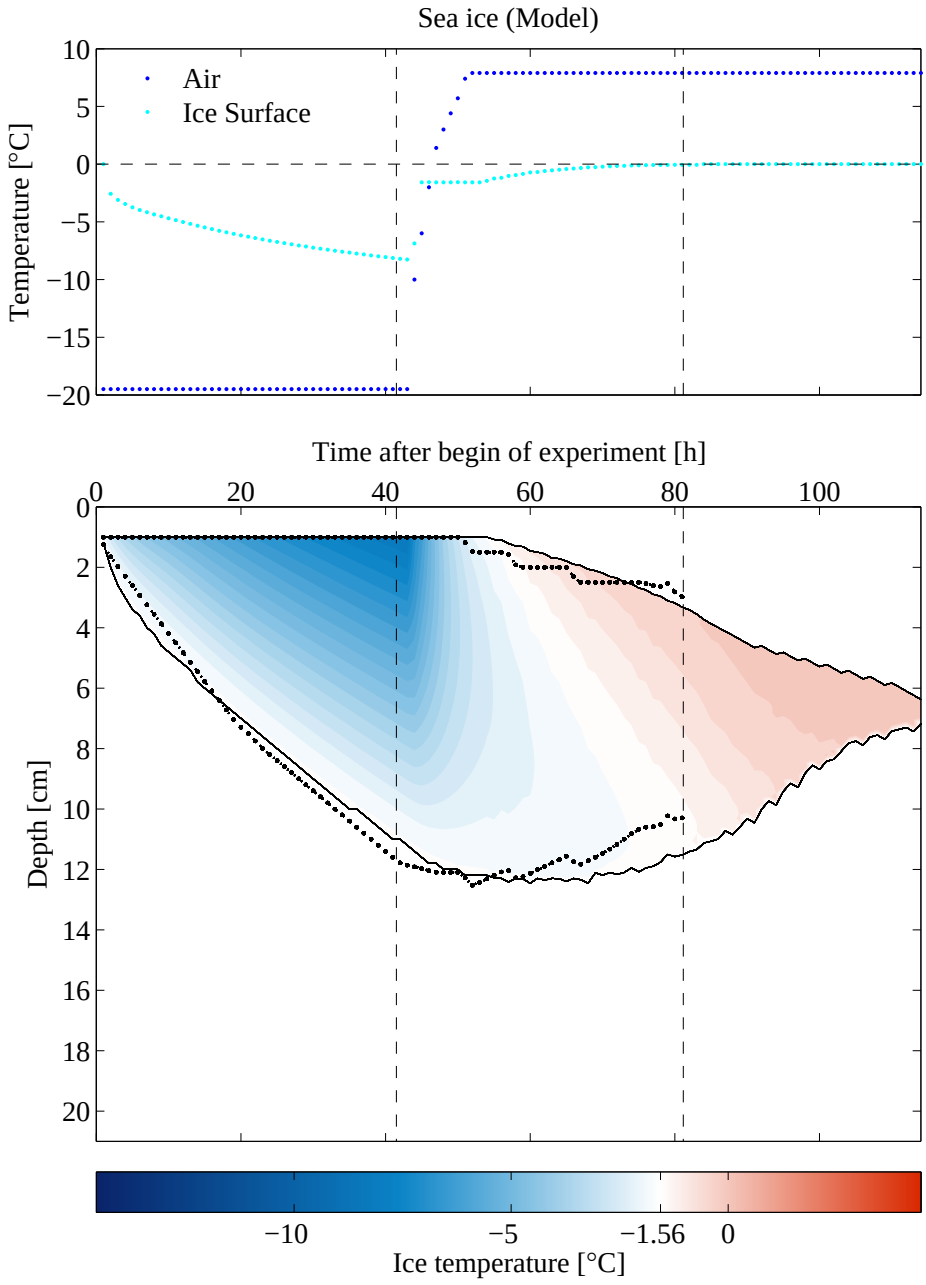

Figure 4.14: *Temporal evolution of the air temperature, ice-surface temperature and internal ice temperature during growth and melting of sea ice (modelled Experiment 5). The black solid lines indicate the modelled ice surface and bottom. The black dotted lines indicate an hourly mean of the measured ice surface and bottom. The first black dashed line indicates the time when the air temperature was switched. The second black dashed line indicates the time when the themistor chain in the laboratory experiment became ice-free. White areas indicate the freezing point of the water.*

The modelled sea-ice temperature shows a slow und non-uniform warming, which was measured in the laboratory experiments as well. However, the warming takes longer in the model, even with consideration of the discontinuous air temperature change. The temperature profile within the ice is non-linear, especially during the first hours after the air temperature was set to higher values (Figure 4.15 (b)). As shown in Figure 4.12, this temperature profile allows heat conduction into the ice and hence a further warming of the ice. The evolution of the ice surface and the bottom height is similar to the measurements. The height of the sea-ice surface decreases similar to freshwater ice. The height of the sea-ice bottom reveals much stronger changes than the freshwater-ice bottom. At first, the rise of the bottom increases with time after the maximum ice thickness is reached. This increase is due to the increasing ice temperature which decreases the solid fraction of the ice and thus simplifies the melting. During the last ten hours the sea ice becomes completely fresh due to flushing, which is indicated by the consistent temperature of 0 °C. This freshening of the ice is also visible in the modelled bulk salinity (Figure 4.16 (b)). Accordingly, the height of the ice bottom changes similarly to freshwater ice, which means a deceleration of the bottom rise. The changes in the sea-ice bottom are consistent with the changes in the melt rate. As the ice temperature increases, the bottom melting and the melt rate increases. After some time the freshening of the sea ice reduces the bottom melting so that the melt rate decreases. Thus, the maximum of the melt rate occurs at the maximum bottom melting. Since the ice completely melted earlier in the laboratory measurements than in the model, the freshening of the ice seems to be less strong in reality.

The model seems to work well for reproducing the laboratory experiments. Therefore, the model is used to analyse the ice's bulk salinity from Experiment 5, since the bulk salinity was not measured during that experiment, but it is an important property of the ice. During ice growth, the typical c-shape profile develops with higher bulk salinities in the upper and lower part of the ice (Figure 4.16 (a)). After the air temperature was set to higher values, at first, the bulk salinity decreases in the upper part of the ice (Figure 4.16 (b)). As a result, the c-shape becomes less distinct. As time goes by, the bulk salinity also decreases deeper in the ice, which eventually results in a continuously increasing bulk salinity from top to the bottom of the ice. At the end of the experiment, the ice becomes completely fresh.

As already pointed out in Section 2.3, the melting temperature of sea ice depends on the bulk salinity and can be calculated with a linear fit of the liquidus relationship (Equation 2.8). Figure 4.17 (a) shows this calculated melting temperature with depth. As expected from the bulk-salinity profile during melting, the melting temperature is highest in the upper and lower part of the ice. Since the bulk salinity decreases with time over the whole depth of the ice, the melting temperature does the same. Figure

4.17 (b) shows the difference between the melting point and the actual temperature of the ice. In contrast to freshwater ice, the temperature of sea ice in not at the melting point over the whole depth. The melting temperature is only reached at the top and the bottom. At the end of the experiment, the whole ice is at the melting point corresponding to the freshening of the ice.

The ice-surface temperature in the model is the temperature of the first layer during ice growth and the melting point during melting. During ice growth the ice-surface temperature is several degrees higher in the model than in the measurements of Experiment 5. During melting the modelled ice-surface temperature is lower than measured in the experiments. The measured ice-surface temperatures during ice growth and melting will be analysed in more detail in the following section.

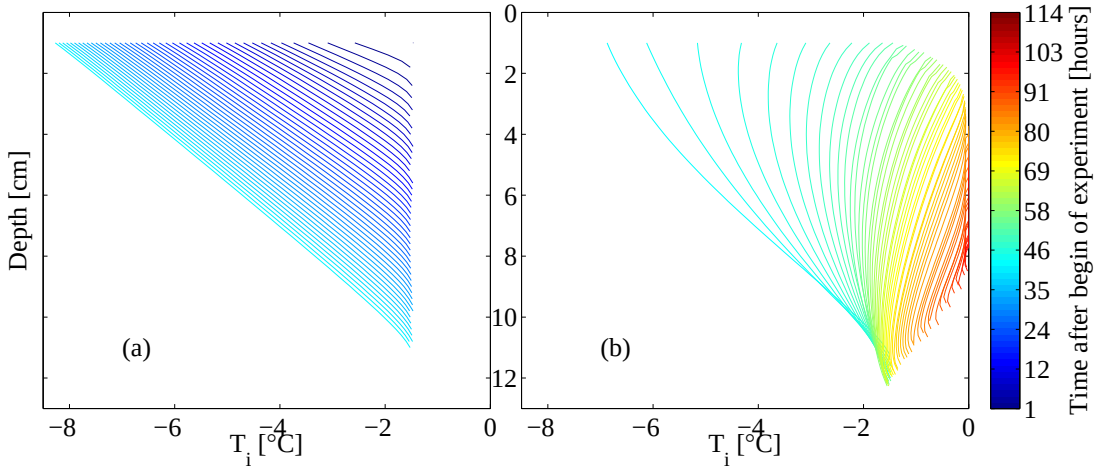

Figure 4.15: *Temporal evolution of the modelled ice temperature profile during ice growth (a) and melting (b).* T_i *corresponds to the ice temperature.*

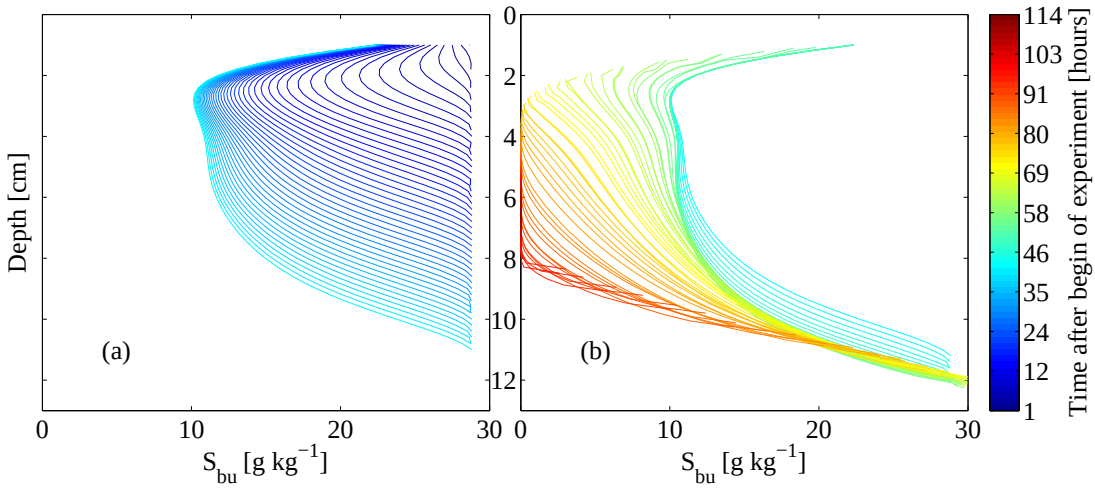

Figure 4.16: *Temporal evolution of the modelled bulk-salinity profile during ice growth (a) and melting (b).* S_{bu} *corresponds to the bulk salinity.*

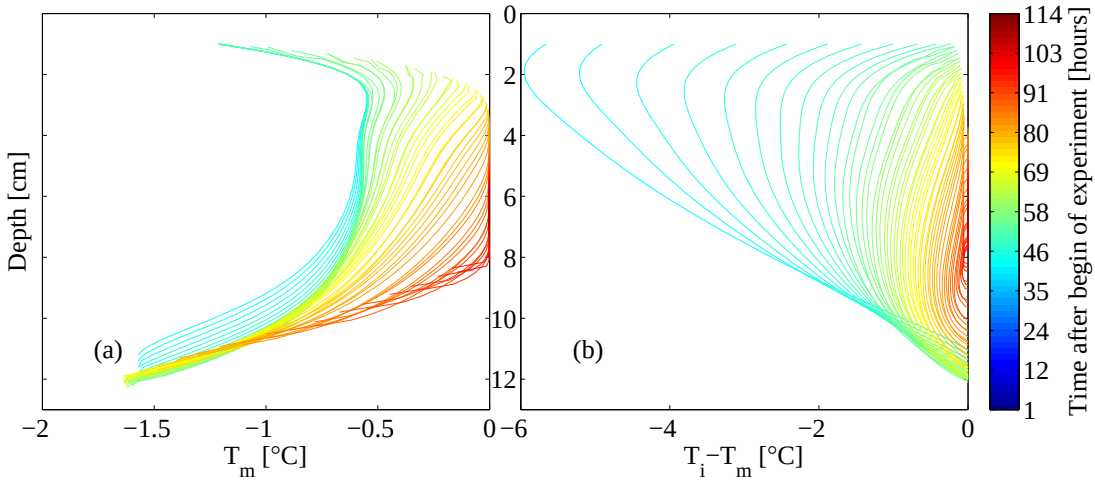

Figure 4.17: *Temporal evolution of the modelled melting point* T_m *of the ice (a) and the difference between the melting point* T_m *and the actual ice temperature* T_i *during melting (b).*

4.3 Ice-surface temperature

In this section the ice-surface temperature during ice growth and melting is analysed in detail. At first, the general structure of the ice surface during growth and melting will be described. Then, a possible dependency of the ice-surface temperature on the initial water salinity and the air temperature during ice melting will be analysed in Section 4.3.1. In Section 4.3.2, the measured ice-surface temperature as a function of ice thickness is compared to a simple approach for calculating the ice-surface temperature out of the ice thickness by assuming a linear ice-temperature profile. Moreover, a dependency of the ice-surface temperature on the initial water salinity and the air temperature during ice growth is investigated.

During ice growth the ice surface was in general smooth. In some experiments (3, 14, 15, 16, 17, 18), frost flowers grew on the ice surface. They started to grow 3 to 12 hours after the experiment began. Frost flowers can form on newly grown ice in a supersaturated water vapour layer and can have a nearly three times higher salinity than the ocean water (*Rankin et al.*, 2002). Figure 4.18 (a) shows a photo of frost flowers in the laboratory. During Experiment 14, an intense frost-flower growth took place, which is clearly visible on the infrared-camera picture (Figure 4.18 (b)). The surface temperature of the frost flowers is several degrees lower than of the pure ice surface. During the other experiments with frost-flower formation less frost flowers grew on the ice surface.

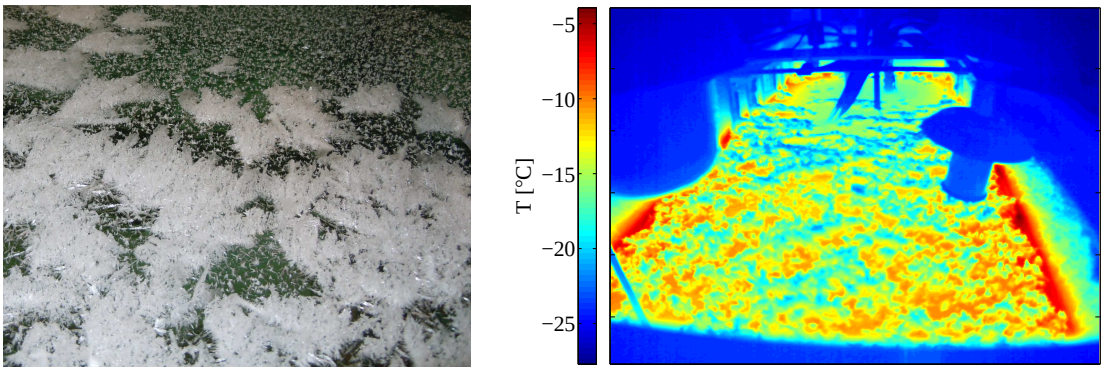

(a) (b)

Figure 4.18: *Frost flowers on the ice surface during Experiment 14: photo (a) and infrared-camera picture (b).* T *is the temperature measured by the infrared camera.*

When Arctic sea ice melts, often melt ponds form on top of the ice. Melt ponds can be found on thick multiyear ice with an uneven surface. There, meltwater from snow and ice can accumulate in depressions of the ice surface (*Fetterer and Untersteiner*, 1998). In the laboratory, such a melt-pond formation was not observed. Nevertheless, small surface irregularities were present on the thin ice grown in the tank, in which very small melt ponds with a diameter of millimeters up to 1 cm could form. Figure 4.19 shows an example of the small accumulations of meltwater on the ice surface when the air temperature was set to 7 °C. At other air temperatures above 0 °C, the ice surface was similar. Inside the cold room, no snow was present that could contribute to the meltwater on the ice surface. However, the frost flowers that grew on the ice surface during some of the experiments were an additional source of meltwater besides the melting sea ice.

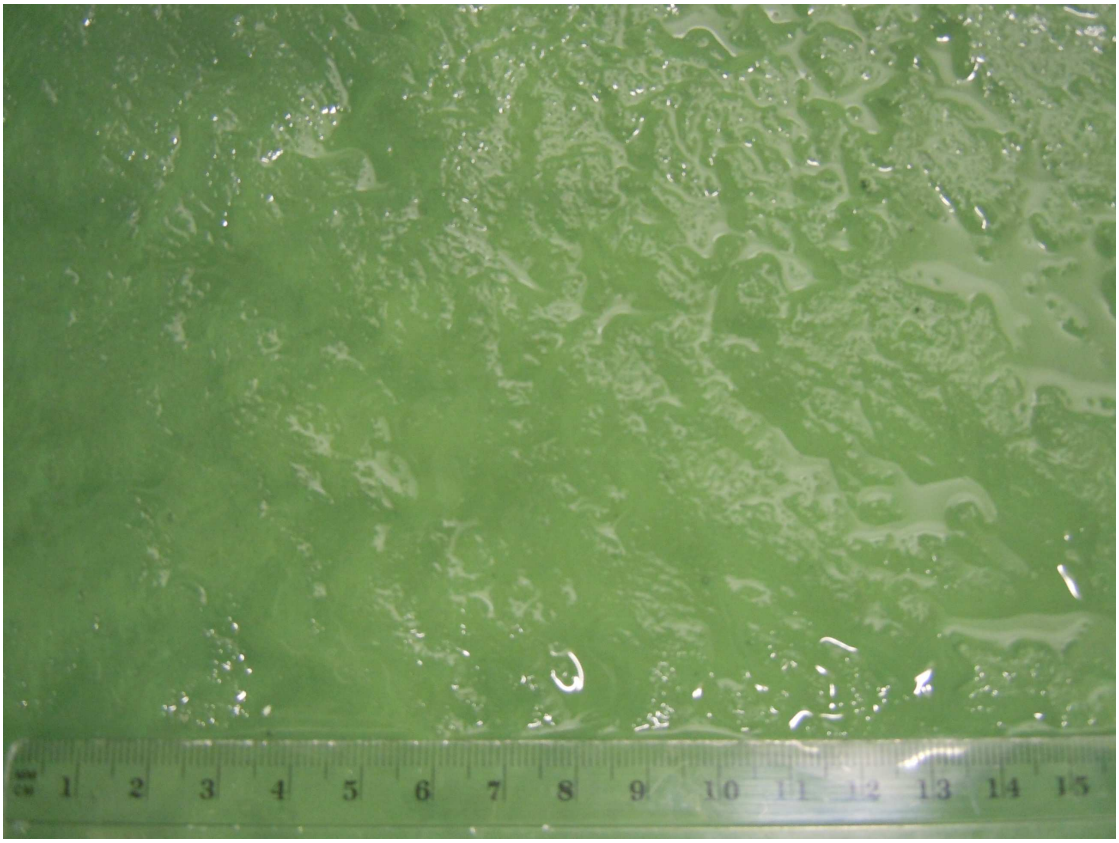

Figure 4.19: *Photo of the ice surface during melting in Experiment 16, when the air temperature was set to 7 °C. The scale of the ruler lying on the ice surface is in centimeters.*

The ice surface temperature was measured with the infrared camera, which took pictures every 30 minutes during the Experiments 3 to 15 and every 15 minutes during the last three experiments. A square of 30 x 30 pixels is chosen in the pictures as the measuring area. The mean temperature in this area is calculated and taken as the ice-surface temperature in the following analysis. Figure 4.20 shows an example of the position of the measuring area in an infrared-camera picture. The square is chosen to be preferably in the middle of the ice surface to prevent any influences from the tank sides, for example from the heating plates intalled there. The position of the square should additionally allow measurements of the ice-surface temperature as long as possible. The measurement ended, when not only ice was in the square, but also water. Thus, for example during Experiment 12 the position was changed between growth and melting, since the ice was partly flooded with water during melting. Hence, the square was placed in the middle of the ice during growth and was shifted closer to the front tank wall during melting. Furthermore, frost flowers are avoided inside the square, which was not possible during Experiment 14 and 17 due to intense frost-flower growth all over the ice surface. During the first period of experiments, the square was mainly placed as shown in Figure 4.20. Due to more instruments and place needed for ice cores during the second period of experiments, the square was shifted a bit closer to the infrared camera into the left side of the tank.

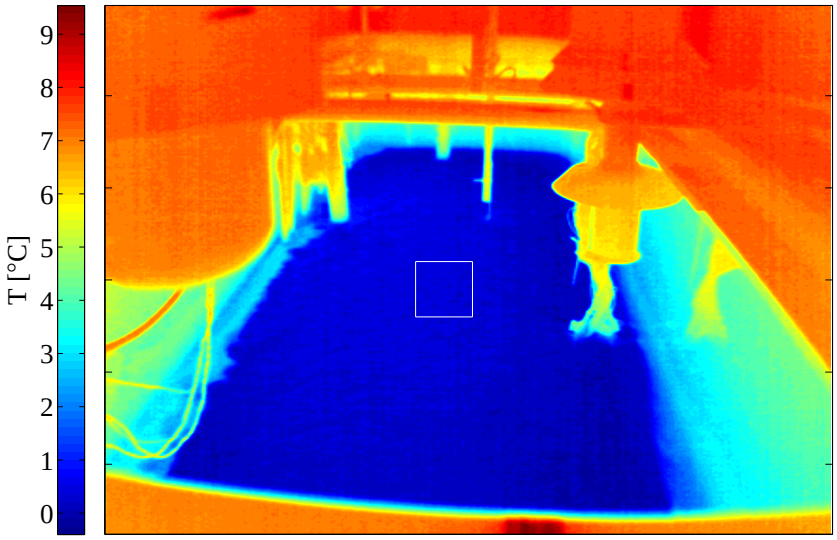

Figure 4.20: *Example of an infrared-camera picture showing the measured surface temperature T during Experiment 11, eleven hours after the air temperature was set to melting conditions. The white square indicates the measuring area.*

4.3.1 Ice melting

During melting the ice surface temperature should be at the melting point, which depends on the bulk salinity of the ice, as already discussed in Section 2.3. Figures 4.10 and 4.11 show that the measured ice-surface temperature was unexpectedly high during Experiment 3 and 5. The values exceeded 0 °C for both freshwater ice and sea ice. Actually, for freshwater ice the surface temperature should be maximum at 0 °C. For sea ice the surface temperature should be even lower due to its salinity. In the following, a dependency of the ice surface temperature on the salinity is investigated in more detail. Furthermore, it is analysed whether, and if so how, the ice-surface temperature depends on the air temperature during melting.

To analyse the dependency of the ice-surface temperature on the salinity, data of experiments with different water salinities are chosen that were performed similarly in order to make a comparison possible. From the first period of measurements, the Experiments 3, 4, 5, 9, 11 and 18 are taken. Thus, data from ice grown out of water with salinities of 0, 12 and 28 g kg^{-1} are available. In the six chosen experiments, 10 cm thick ice was grown and subsequently melted at a set air temperature of 10 °C. In order to have one more salinity covered in the analysis, Experiment 12 with a water salinity of 33 g kg^{-1} from the second period of measurements is chosen. This experiment was conducted under conditions comparable to the six experiments from the first period. The main difference is the stepwise increase of the air temperature. It is not possible to take more data from the second period of measurement for different reasons. First of all, the air temperature was set to different values during melting than in the first period of measurements (Table 3.2). In Experiment 13 the ventilator was turned off most of the time, whereas the ventilator was turned on the whole time during melting in all the other experiments. From Experiment 17 there is not enough data available of the time when the air temperature was set to 10 °C.

Figure 4.21 shows the ice surface temperature as a function of the initial water salinity. Information on the bulk salinity at the time of melting is not available. Sea ice loses salt both during growth and melting due to processes like gravity drainage and flushing so that the bulk salinity decreases with time. Nevertheless, it can be assumed, that the higher the initial water salinity is, the higher the bulk salinity of the ice is. For the analysis, ice-surface temperatures are first taken four hours after the air temperature inside the cold room reached 0 °C, since some time is needed for the air temperature to reach the mean value during melting and for the ice surface to adapt to the new air temperatures. For experiments with the same initial water salinity (Exp. 5, 9 and 11 with 28 g kg^{-1} and Exp. 3 and 18 with 0 g kg^{-1}) a mean of the measured initial water salinity and all the relevant ice-surface temperatures is calculated. Moreover, the standard deviation is

calculated as follows:

$$SD = \sqrt{\frac{1}{n-1}\sum_{i=1}^{n}(x_i - \overline{x})^2}$$

$\overline{x}$ is the mean of the measurements x_i. The number of measurements n differs between initial water salinities. Since for some initial water salinities data from several experiments are available, while for other initial water salinities only data from one experiment can be taken for this analysis, n varies between 65 and 221.

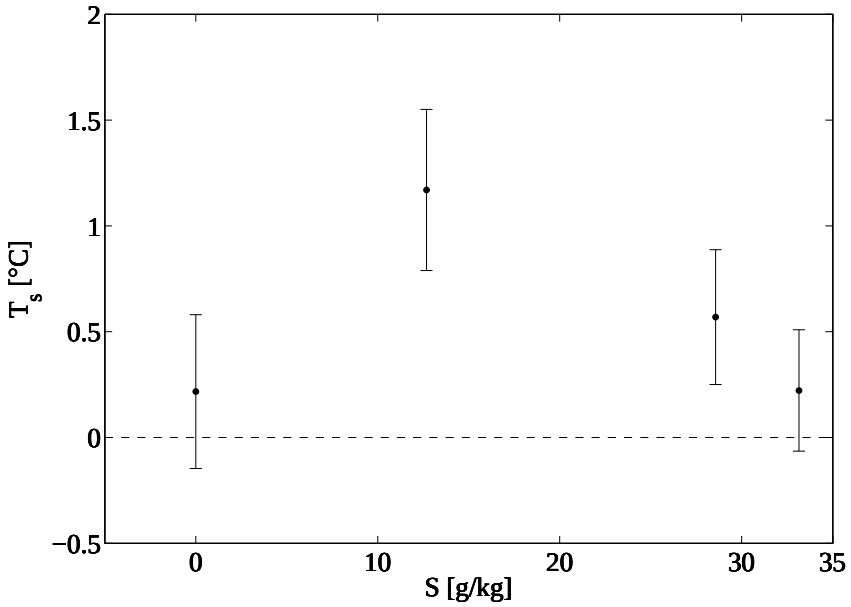

Figure 4.21: *The ice-surface temperature T_s as a function of the initial water salinity S the ice was grown out of.*

Figure 4.21 shows that the measured ice-surface temperature is unexpectedly mainly above 0 °C, independent of salinity. Especially during Experiment 4 the surface temperature is very high with a mean temperature above 1 °C. Due to salt loss of sea ice the melting point of the ice is higher than the freezing point of the water the ice was grown out of, but nevertheless the melting point and thus the ice-surface temperature should be below 0 °C. At first, a clear dependency of the ice-surface temperature on the initial water salinity is not obvious. Neglecting the freshwater ice, the ice-surface temperature decreases with an increasing initial water salinity likely due to a higher bulk salinity.

Since the ice-surface temperature during melting has so far only been analysed at the same set air temperature, the ice-surface temperature as a function of the air temperature is investigated next. Again, comparable experiments are chosen. From the first period of measurements, Experiments 8 and 10 were added to the others chosen previously, since during those experiments the air temperature was set to 5 °C and 15 °C respectively. The second period of measurements gives more data due to the stepwise increase of the air temperature. All periods are chosen during which the air temperature was set to values above the melting point of sea ice. For the analysis data is taken four hours after an air-temperature switch until the next one or the end of the experiment if it is the last change in air temperature. Furthermore, the data is separated by salinities. Freshwater ice was not melted at air temperatures other than 10 °C, so that no freshwater experiments are included in this analysis. Comparable to the previous analysis, the mean of the relevant air and ice-surface temperatures and the standard deviation is calculated.

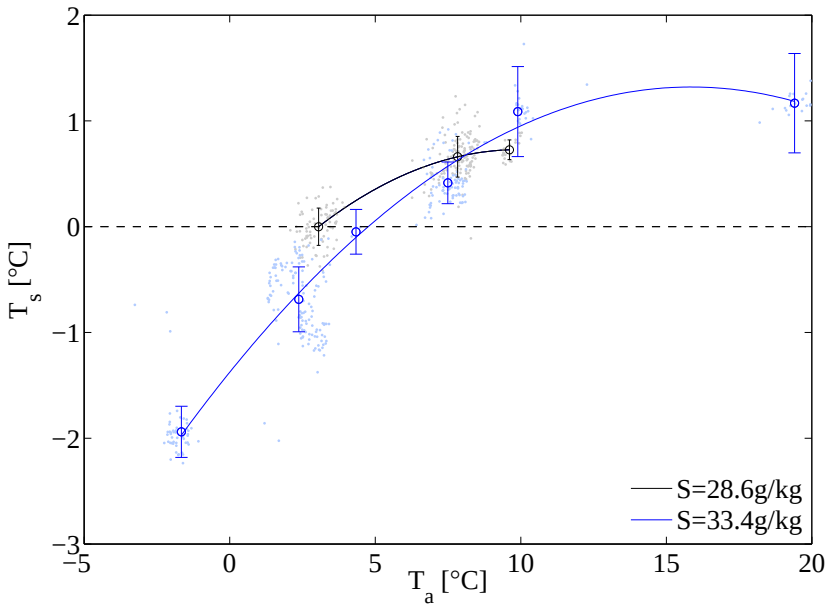

Figure 4.22: *The ice-surface temperature T_s as a function of the initial water salinity S and the air temperature T_a during melting.*

Figure 4.22 shows the ice-surface temperature as a function of the air temperature during melting. The ice-surface temperature increases with increasing air temperature, independent of salinity. A second degree polynomial was fitted to the measurements. For the higher salinity of 33.4 g kg^{-1}, this increase is steeper than for the lower salinity. At

air temperatures above 5 °C the ice-surface temperature has values above 0 °C which is considerably higher than expected. A reason for these high surface temperatures could be found in the structure of the ice surface. Possibly, the meltwater in the small melt ponds could warm above the melting point, which contributes to the measured surface temperature.

4.3.2 Ice growth

After looking at the ice-surface temperature during melting, the ice-surface temperature during ice growth is analysed in this section. Not only a dependency of the ice-surface temperature on the initial water temperature and the air temperature is anlysed, but also an ice-thickness dependency. Therefore, experiments from both periods of measurements are chosen, during which the ice was grown at the same set air temperature out of water with different initial salinities. These are all experiments from the first period of measurements, except for Experiment 3 and 10. During these two experiments the ice-surface temperature was not measured during ice growth. The infrared camera was first installed shortly before the melting started in Experiment 3 and the camera stopped taking pictures for unknown reasons during Experiment 10. The experiments from the first period of measurements include the initial water salinities 0, 12 and 28 $g\,kg^{-1}$. During those experiments, the ice was grown at an air temperature of -20 °C. From the second period of measurements Experiment 12 and 13 are chosen for the analysis, since the ice was grown under the same conditions as in the experiments of the first period of measurements. It has to be kept in mind that the ventilator was turned off during ice growth in Experiment 13. As mentioned before, the cooling of the cold room had to warm up approximately every six hours in order to defrost. These defrosting periods are cut out of the data and discussed separately. Even though the ice might not be in thermal equilibrium during the defrosting periods, the data are used to analyse the surface temperature at a higher air temperature.

Figure 4.23 shows the surface temperature as a function of ice thickness for different air temperatures and initial water salinities. Due to the fact that ice is a good thermal insulator, the ice-surface temperature strongly depends on the ice thickness. The surface temperature decreases nearly linearly with an increasing ice thickness, independent of salinity. For all sea ice types the ice-surface temperature is 2 °C lower than for freshwater ice. This is the case for both air temperatures. This difference is probably caused by the lower freezing point of seawater. Furthermore, the ice-surface temperature is around 2 °C lower, when the ventilator is turned off at -19 °C air temperature. During the defrosting periods, the difference is only around 1 °C. The slope of the nearly linear relationship between surface temperature and ice thickness is steeper compared to the

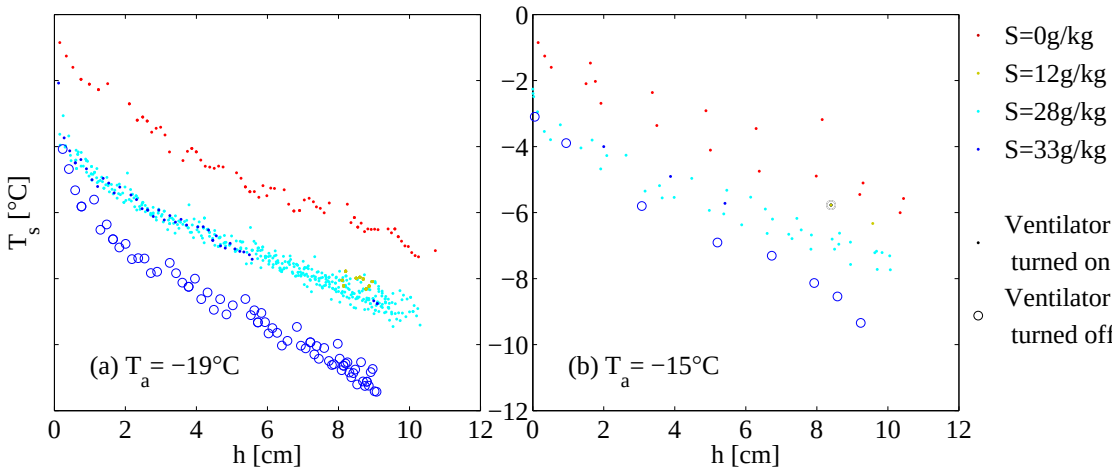

Figure 4.23: *The ice surface temperature T_s as a function of the ice thickness h and the mean air temperature T_a during growth: at an air temperature of -19 °C (a) and during the defrosting periods of the cold room (b).*

experiments with the ventilator being turned on.

During ice growth, the ice-surface temperature can be calculated from the ice thickness. To do so, thermal inertia is assumed to be zero, which results in a linear ice-temperature profile. Consequently, the conductive heat flux in the ice Q_c equals the atmospheric heat flux Q_a (Section 2.3). The ice-surface temperature can then be calculated as follows:

$$\begin{aligned} Q_c &= Q_a \\ k_i \frac{T_f - T_s}{h} &= C(T_s - T_a) \\ T_s &= \frac{k_i T_f + hCT_a}{hC + k_i} \end{aligned} \tag{4.2}$$

T_f corresponds to the freezing point of the water underneath the ice and thus T_f is the ice temperature at the bottom, T_s corresponds to the ice-surface temperature, T_a to the air temperature, h to the ice thickness, k_i to the heat conductivity of ice and C to the heat transfer coefficient. Figures 4.10 and 4.11 show that the ice temperature profile is linear during ice growth and thus, this assumption is justified.

The calculation of the ice-surface temperature with Equation 4.2 is compared to the measured data in Figure 4.24 and Figure 4.25. First, the calculation is done for a freshwater-ice experiment (Exp. 18), during which surface-temperature measurements

were done during ice growth. The measured air temperature and ice thickness are inserted into Equation 4.2. The advantage of freshwater ice is that the heat conductivity is exactly known (2.2 W m^{-1} K^{-1}). For sea ice the heat conductivity strongly depends on the bulk salinity and the ice temperature (Figure 2.2 (b)). Hence, only the heat transfer coefficient is unknown for freshwater ice. *Naumann* (2011) calculated the heat transfer coefficient during sea-ice experiments performed in the same tank inside the same cold room as used for this study. Her estimates of the heat transfer coefficient vary between 14.8 W m^{-2} K^{-1} and 27.1 W m^{-2} K^{-1}. The mean value was 20 W m^{-2} K^{-1}. Thus, the surface temperature of freshwater ice is calculated with two different heat transfer coefficients to see which one gives the better results compared to the measurements. The results are presented in Figure 4.24. A calculation of the surface temperature with C = 10 W m^{-2} K^{-1}, which is half of the mean value calculated by *Naumann* (2011), is most similar to the measurements. The slope of the almost linear dependency is the same, but on the other hand, the calculated temperature is 1 °C higher than the measured temperature. This difference might come from frost flowers that grew on the ice during Experiment 18. With C = 20 W m^{-2} K^{-1} the surface temperature is underestimated increasingly with increasing ice thickness larger than 2 cm. At 10 cm thick ice, the calculation gives already a 2 °C lower temperature than measured.

Looking at all other experiments, C = 10 W m^{-2} K^{-1} gives better results than C = 20 W m^{-2} K^{-1}. Therefore, for the following calculations, C = 10 W m^{-2} K^{-1} is used. To compare the calculated sea-ice surface temperatures to the measurements, the heat conductivity of the sea ice is required. Since the bulk salinity is unknown, the calculation is done again with two estimated values for the heat conductivity to see which one fits best. From the wide range of sea-ice experiments that were performed, Experiment 5 is chosen, since during this experiment both ice thickness and surface temperature were measured close to each other, like in Experiment 18. Moreover, this experiment is already included into most of the analysis of the data in the previous sections. Figure 4.25 (a) shows the results of the calculation of the surface temperature. With a heat conductivity closer to the heat conductivity of freshwater ice, the nearly linear dependency between the ice thickness and the ice-surface temperature is best obtained. On the other hand, the calculated surface temperature is around 2 °C higher than the measured temperature. During Experiment 5 frost-flower growth was not observed, which could have explained this difference between the calculation and the measurement. With a heat conductivity half of the heat conductivity of freshwater ice, the slope is much steeper so that the surface temperature is first overestimated until 4 cm of ice is reached and afterwards the surface temperature is underestimated.

The two previous analysed experiments show that the surface temperature of sea ice is calculated best out of the sea-ice thickness with C = 10 W m^{-2} K^{-1} and k_i =2 W m^{-1} K^{-1}.

Just a continuous offset of 1 °C to 2 °C occurs, but the slope of the dependency is like measured. With these conclusions the calculation of the ice-surface temperature of thicker ice is finally tested. Therefore, Experiment 17 from the second period of measurements is taken, since during this experiment the thickest ice was grown. In general, the calculation reproduces the measurements quite well with an offset of some °C. During this experiment, again frost flowers grew on the ice surface which very likely have an effect on the measured surface temperature. When the ice became thicker than 10 cm, the measured ice-surface temperature decreased more slowly with increasing ice thickness than calculated.

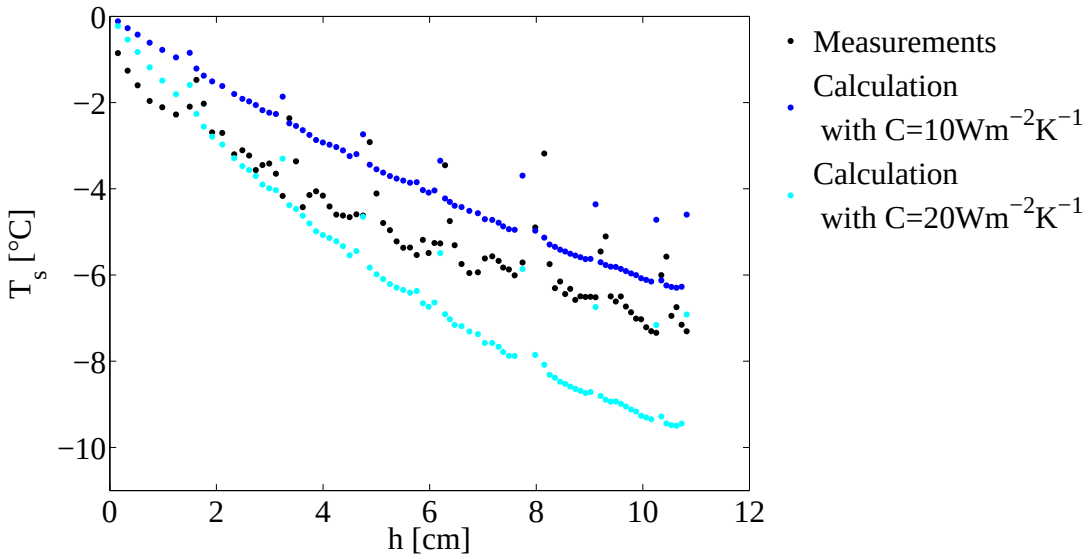

Figure 4.24: *The ice-surface temperature T_s as a function of the ice thickness h. Measurements and calculations from a freshwater-ice experiment (Exp. 18). C corresponds to the heat transfer coefficient.*

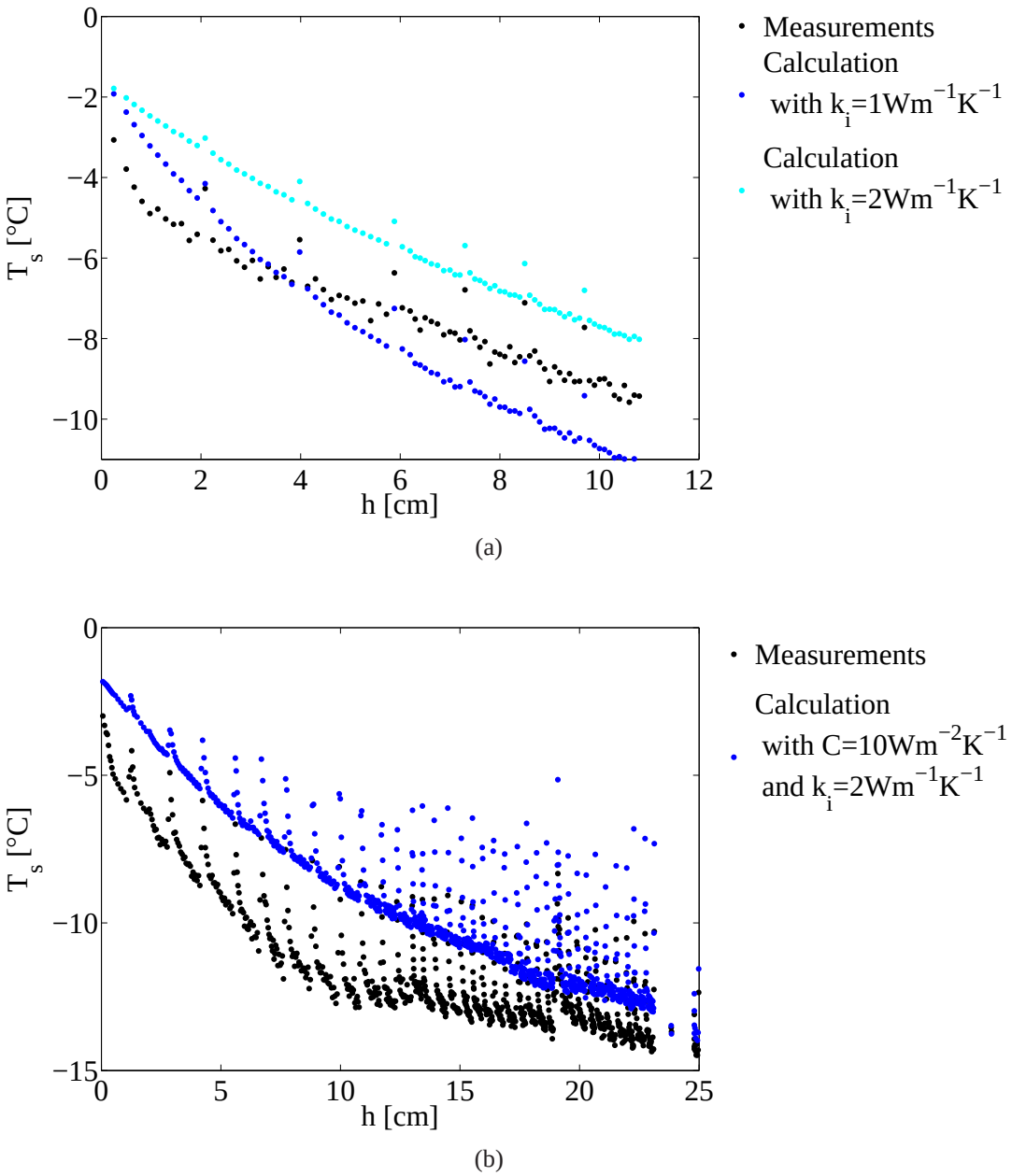

Figure 4.25: *The ice-surface temperature T_s as a function of the ice thickness h. Measurements and calculations from two sea-ice experiments (Exp. 5, (a), and Exp. 17, (b)). For the calculations in Experiment 5, the heat transfer coefficient C is set to 10 W m^{-2} K^{-1}. k_i corresponds to the heat conductivity of the ice.*

Chapter 5

Summary and outlook

5.1 Summary

Tank experiments were performed to analyse the thermodynamics of melting sea ice. Sea ice and freshwater ice was compared to clarify the influence of the salt within sea ice. The laboratory experiments were partly extended with model experiments. The study focused on the investigation of the melt rate, the internal ice temperature and the ice-surface temperature during melting.

Melt rate
The laboratory measurements reveal that sea ice melts faster than freshwater ice. Moreover, sea ice melts faster in turbulent water than in calm water. At a constant air temperature the melt rate of freshwater ice is constant with time, whereas the melt rate of sea ice shows a distinct maximum. As sea ice gets warmer, the solid fraction decreases due to the internal melting which accelerates the melting of sea ice. Hence, the melt rate of sea ice increases with time. The applied thermodynamic sea-ice model can reproduce the measured melt rates. Further model experiments show that the maximum in the melt rate of sea ice occurs earlier at a higher atmospheric heat flux. Independent of salinity, the ice grows and melts faster at a higher atmospheric and oceanic heat flux. At a cer-

tain atmospheric heat flux the ice exists longer than at higher or lower atmospheric heat fluxes.

Internal ice temperature

During ice growth a linear temperature profile established both in freshwater ice and in sea ice. After changing the air temperature to melting conditions, the freshwater ice warms faster than sea ice, since a sea-ice warming requires more energy due to internal melting. Freshwater ice warms uniformly up to the melting point over the whole depth. Thus, there is no temperature profile present within the ice. The surface melting of freshwater ice is stronger than the bottom melting since the atmospheric heat flux is higher than the oceanic heat flux. In sea ice a non-linear temperature profile evolves during melting. This temperature profile allows heat conduction within the ice. Thus, the energy of the atmospheric and oceanic heat flux that is not required for melting at the surface and bottom is conducted into the ice and further warms the inner ice. The bottom melting of sea ice is stronger than bottom melting of freshwater ice. Due to the bulk-salinity profile within the sea ice, the solid fraction decreases with depth. Thus, bottom melting of sea ice does not require as much energy as for freshwater ice. This effect increases as the ice temperature increases and hence the solid fraction decreases. The increasing bottom melting fits well to the increase in the melt rate. During one of the sea-ice experiments, a flushing event was very likely observed by a sudden and temporary temperature increase in the upper two thirds of the ice.

Ice-surface temperature

The ice surface was smooth during ice growth. In some experiments, frost flowers grew on the ice, which had a lower surface temperature than the pure ice. Due to the fact that ice is a good thermal insulator, the ice-surface temperature strongly depends on the ice thickness during growth. The surface temperature decreases nearly linearly with increasing ice thickness, independent of salinity. The surface temperature of sea ice is 2°C lower than of freshwater ice, likely due to the lower freezing point of seawater. The surface temperature can be calculated out of the ice thickness assuming a linear temperature profile within the ice. This assumption is justified since the laboratory measurements show a linear ice-temperature profile during ice growth. A heat transfer coefficient of 10 $W\,m^{-2}\,K^{-1}$ and a heat conductivity of 2 $W\,m^{-1}\,K^{-1}$ are found to be the best values to calculate the measured surface temperature of sea ice. The slope of the nearly linear dependency is reproduced well, but the calculated surface temperature is 1°C to 2°C higher than the measured surface temperature. This difference might result from frost-flower growth. During melting, very small melt ponds formed in small irregularities of the ice surface. The meltwater originated from melted ice and frost flowers. The ice-surface temperature is unexpectedly well above the melting point of the ice, independent of salinity. Such high temperatures are possibly caused by the small melt ponds

which maybe warmed up above the melting point. Neglecting the freshwater ice, the ice-surface temperature decreases with an increasing initial water salinity likely due to a higher bulk salinity of the ice and thus a lower melting point. Moreover, the surface temperature of sea ice increases with an increasing air temperature.

5.2 Outlook

The performed laboratory experiments were the first ones to investigate the melting of sea ice. A first impression of what happens during the melting of sea ice is received. But there are still some open questions that arose from of the obtained results. To answer the questions further laboratory experiments are required. Moreover, some improvements can be done in future laboratory experiments on melting sea ice.

Open questions

Melt rate:

- In the laboratory experiments, sea ice melted faster when the pumps were turned on. An assumption is that the energy from the pumps and from the heating wire around the pumps caused the faster melting. Therefore, two experiments with turned on pumps were modelled with the thermodynamic model, in which the oceanic heat flux was set to a higher value than in the laboratory experiments to take into account the additional heat from the pumps. To reproduce the measured ice thickness evolution well, the oceanic heat flux had to be increased far beyond the possible additional heat from the pumps. What happens with melting ice in turbulent water?
- The melt rate was only investigated for 10 cm thick ice. Sea ice in the Arctic and Antarctic is usually thicker than 10 cm. How does the melt rate evolve for thicker ice? Does relatively fresh and thick multiyear ice melt similar to freshwater ice?

Internal ice temperature:

- The cold room has to warm up approximately every six hours to defrost. This temperature signal penetrates into the ice over the whole depth. Such regular and strong warming periods are rather unusual in nature. Consequently, the ice grown inside the cold room might differ from naturally grown ice. How do these defrosting periods influence the ice? Does this warming for example have an impact on the ice's salinity?
- In one experiment, a flushing event was probably observed. Within some hours the ice temperature increased up to 0°C and decreased again in the upper two thirds of the ice. Did this flushing occur naturally or was it caused by the thermistor chain? Is it

possible to measure such a flushing event in the field? How deep does such a flushing event usually penetrate into the ice?

Ice-surface temperature:

- During ice growth, the surface temperature of sea ice was roughly 2°C lower than of freshwater ice, independent of salinity. This difference might come from the lower freezing point of seawater. But why does the difference not vary between sea ice with different salinities?
- During melting the surface temperature of sea ice increases with an increasing air temperature. Is this also valid for freshwater ice? The increasing surface temperature of sea ice might be explained with a warming of the small melt ponds on the sea-ice surface. The small melt ponds and the pure ice surface could not be distinguished on the infrared-camera pictures taken during these experiments. Pictures should be done closer to the ice surface to measure the surface temperature of the small melt ponds. Is the temperature of the melt ponds really higher than of the pure ice?
- The bulk salinity of sea ice changes during melting, which was not considered in the analysis of the ice-surface temperature. How does the ice-surface temperature depend on the bulk salinity?

Improvements of the experimental setup

Ice-thickness measurements:
A convenient improvement would be automatical ice-thickness measurements. First, the measurements would be continuous and gaps due to the night would not occur. Second, variations in ice thickness measurements done by different people looking differently at the ruler can be avoided. A realization of automatical ice thickness measurements is not found yet. One possibility might be the installation of a webcam. But then a parralax-free view should be ensured by moving the camera as the ice grows. This movement should be of course somehow automatically as well. Additionally, a fogging of the camera has to be avoided.

Ice-temperature measurements:
The thermistor chains conduct heat into the ice, which influences the ice around the chain both during growth and melting. The ice grows fast and funnel-shaped around the thermistor chain so that the ice is some centimeters thicker there compared to the remaining ice in the tank. At high air temperatures the heat conduction leads to ice melting around the thermistor chain. Thus, the ice temperature can not be measured during the end of the melting. The heat conduction of the thermistor chain should therefore be avoided or at least reduced in future sea-ice experiments. A solution could be to build smaller thermistor chains that let the thermistors stick out some cm into the ice so that

they are not affected by the chain.

Free floating ice:
Despite the heating plates around the tank, the ice froze on the walls of the tank and was not afloat in some of the laboratory experiments. The ice also froze around the frame on which the CTDs were installed. Especially during melting the ice should be afloat since due to surface melting the ice surface easily gets below the water surface when the ice is fixed so that the ice gets flooded with water. An installation of stronger heating plates, maybe on the inner side of the tank wall might prevent the ice from freezing on the walls and the CTD frame. A different installation of the CTDs without the frame can be considered as well. Attention must be paid to all other fixed instruments in the tank. For example the ice should not freeze around the fixed CTDs, which will hold the ice down. Instruments deployed in the ice, like the thermistor chains, should have a counterweight so that the instruments can easily move with the ice and do not press the ice down.

Bibliography

Buettner, K. and Kern, C. (1965). The determination of infrared emissivities of terrestrial surfaces. *Journal of Geophysical Research*, 70(6):1329–1337.

De La Rosa, S., Maus, S., and Kern, S. (2011). Thermodynamic investigation of an evolving grease to pancake ice field. *Annals of Glaciology*, 52(57):206–214.

Eicken, H., Krouse, H. R., Kadko, D., and Perovich, D. K. (2002). Tracer studies of pathways and rates of meltwater transport through arctic summer sea ice. *Journal of Geophysical Research*, 107.

Eisen, O. and Kottmeier, C. (2000). On the importance of leads in sea ice to the energy balance and ice formation in the weddell sea. *Journal of geophysical research*, 105(C6):14045–60.

Feltham, D. and Worster, M. (2000). Similarity solutions describing the melting of a mushy layer. *Journal of crystal growth*, 208(1):746–756.

Feltham, D. L., Untersteiner, N., S.Wettlaufer, J., and Worster, G. (2006). Sea ice is a mushy layer. *Geophysical Research Letters*, 33(L14501).

Fetterer, F. and Untersteiner, N. (1998). Observations of melt ponds on arctic sea ice. *Journal of Geophysical Research*, 103(C11):24821–24.

Fofonoff, N. and Millard, R. (1983). Algorithms for computation of fundamental properties of seawater. *Unesco technical papers in marine science*, 44.

Griewank, P. J. and Notz, D. (submitted). Insights in brine dynamics and sea-ice desalination from a 1d model study of gravity drainage. *Journal of Geophysical Research - Oceans*.

Holt, B. and Digby, S. A. (1985). Processes and imagery of first-year fast sea ice during the melt season. *Journal of Geophysical Research*, 90(C3):5045–5062.

InfraTec (2007). Variocam high resolution Benutzerhandbuch.

Jardon, F., Notz, D., Vivier, F., and Sammonds, P. (in preparation). Brine convection over the entire sea ice thickness: Laboratory experiments.

Leppäranta, M. (1993). A review of analytical models of sea-ice growth. *Atmosphere-Ocean*, 31(1):123–138.

Naumann, A. K. (2011). Physikalische Prozesse der Meereisentwicklung in offenem Wasser. master thesis, Universität Hamburg.

Notz, D. (2005). *Thermodynamic and fluid-dynamical processes in sea ice*. Phd thesis, University of Cambridge.

Notz, D., Wettlaufer, J., and Worster, M. (2005). A non-destructive method for measuring the salinity and solid fraction of growing sea ice in situ. *Journal of Glaciology*, 51(172):159–166.

Rankin, A., Wolff, E., Martin, S., et al. (2002). Frost flowers: Implications for tropospheric chemistry and ice core interpretation. *Journal of Geophysical Research*, 107(4683):10–1029.

Schwerdtfeger, P. (1963). The thermal properties of sea ice. *Journal of Glaciology*, 4(36):789–807.

Serreze, M. and Francis, J. (2006). The arctic amplification debate. *Climatic Change*, 76(3):241–264.

Stössel, A., Yang, K., and Kim, S. J. (2002). On the role of sea ice and convection in a global ocean model. *Journal of Physical Oceanography*, 32(4):1194–1208.

Stroeve, J., Holland, M., Meier, W., Scambos, T., and Serreze, M. (2007). Arctic sea ice decline: Faster than forecast. *Geophysical Research Letters*, 34(9):9501.

Tison, J. L., Worby, A., Delille, B., Brabant, F., Papadimitriou, S., Thomas, D., De Jong, J., Lannuzel, D., and Haas, C. (2008). Temporal evolution of decaying summer first-year sea ice in the western weddell sea, antarctica. *Deep Sea Research Part II: Topical Studies in Oceanography*, 55(8):975–987.

Wadhams, P. (2000). *Ice in the Ocean*. RoutledgeCurzon.

Weeks, W. F. (2010). *On Sea Ice*. University of Alaska Press.

Widell, K., Fer, I., and Haugan, P. M. (2006). Salt release from warming sea ice. *Geophysical research letters*, 33(12).

Acknowledgements

First of all I would like to thank my supervisor Dr. Dirk Notz, who drew my interest in sea ice during my studies on Svalbard and who came up with the topic of this thesis.

Thanks to Prof. Dr. Martin Claußen who was the first supervisor of this thesis and who was a very good mentor during my studies.

Many thanks to Philipp Griewank, who was always there for answering questions and handing out good advises. He also came up with the idea of presenting a poster at the EGU, which was a great and important experience. Moreover, he provided his model SAMSIM for the model studies in this thesis.

I would like to thank Stefanie Arndt, who was a very good assistant during the laboratory experiments.

Thanks to Lutz Hirsch, from whom I could borrow the infrared camera.

Moreover, I would like to thank the staff of the workshop, who helped a lot with constructions for the tank setup.

I would like to thank Ann Kristin Naumann und Iris Ehlert, who helped me a lot with their experience, especially during my first days in the laboratory.

Many thanks to Jessica Engels, with whom I spent many nice lunch and tea breaks and who always kept my spirits up whenever something did not work as planned. Moreover, I would like to say thanks for proofreading.

I would also like to thank Wayne Neely and Thomas Keitzl for proofreading the first version of this thesis.

Special thanks to my father Jürgen Wiese, who always supports me whatever I do and wherever I go.

Erklärung zur Anfertigung und Veröffentlichung der Arbeit

Hiermit erkläre ich, dass ich die vorliegende Arbeit selbstständig verfasst und keine anderen als die angegebenen Hilfsmittel, insbesondere keine nicht genannten Internet-Quellen verwendet habe. Weiterhin versichere ich, dass ich diese Arbeit vorher nicht in einem anderen Prüfungsverfahren eingereicht habe. Die eingereichte schriftliche Fassung der Arbeit entspricht der auf dem Speichermedium.
Einer Veröffentlichung der Arbeit in der Bibliothek der Universität Hamburg stimme ich zu.

Hamburg, den 18. September 2012

_____

Mareike Wiese